Eur. Phys. J. C 10, 271–292 (1999)
Digital Object Identifier (DOI) 10.1007/s100529900084

THE EUROPEAN PHYSICAL JOURNAL C

New analysis of the $\Delta I = 1/2$ rule in kaon decays and the $\hat{B}_K$ parameter

T. Hambye[1], G.O. Köhler[2], P.H. Soldan[2]

[1] INFN – Laboratori Nazionali di Frascati, P.O. Box 13, I-00044 Frascati, Italy (hambye@lnf.infn.it)
[2] Institut für Physik, Universität Dortmund, D-44221 Dortmund, Germany (koehler, soldan@doom.physik.uni-dortmund.de)

Received: 22 February 1999 / Published online: 12 August 1999

Abstract. We present a new analysis of the $\Delta I = 1/2$ rule in $K \to \pi\pi$ decays and the $\hat{B}_K$ parameter. We use the $1/N_c$ expansion in the effective chiral lagrangian for the pseudoscalar mesons and compute the hadronic matrix elements at leading and next-to-leading order in the chiral and the $1/N_c$ expansions. Numerically, our calculation reproduces the dominant $\Delta I = 1/2$ $K \to \pi\pi$ amplitude. Our result depends only moderately on the choice of the cutoff scale in the chiral loops. The $\Delta I = 3/2$ amplitude emerges sufficiently suppressed but shows a significant dependence on the cutoff. The $\hat{B}_K$ parameter turns out to be smaller than the value previously obtained in the $1/N_c$ approach. It also shows a significant dependence on the choice of the cutoff scale. Our results indicate that corrections from higher order terms and/or higher resonances are large for the $\Delta I = 3/2$ $K \to \pi\pi$ amplitude and the ($|\Delta S| = 2$) K^0–$\bar{K}^0$ transition amplitude.

1 Introduction

Over the last few decades the kaon system has provided us with a rich field of phenomenology which has been important for developing our theoretical understanding of the interplay of weak and strong interactions. The non-leptonic kaon decays are especially interesting because they provide a testing ground for QCD dynamics at long distances. Two outstanding problems in the field are the explanation of the $\Delta I = 1/2$ rule in $K \to \pi\pi$ decays and the calculation of the $\hat{B}_K$ parameter which measures the non-perturbative contributions to the ($|\Delta S| = 2$) K^0–$\bar{K}^0$ transition amplitude. An accurate knowledge of $\hat{B}_K$ is necessary for theoretically investigating the indirect CP violation in the neutral kaon mass matrix, as well as the K_L–K_S mass difference. The $\Delta I = 1/2$ rule is particularly important because it gives rise to the small value of the ratio ε'/ε which measures the direct CP violation in the $K \to \pi\pi$ decay amplitudes.

Since its first observation more than 40 years ago [1] the $\Delta I = 1/2$ enhancement has attracted a great deal of theoretical interest in the attempts to find the dynamical mechanism behind the approximate isospin selection rule, in particular within the standard model. Experimentally, the ratio of the $\Delta I = 1/2$ and $\Delta I = 3/2$ amplitudes in $K \to \pi\pi$ decays corresponding to $I = 0$ and $I = 2$ in the final state, respectively, was measured to be

$$\frac{1}{\omega} \equiv \frac{\mathrm{Re}a_0}{\mathrm{Re}a_2} \equiv \frac{\mathrm{Re}(K \to (\pi\pi)_{I=0})}{\mathrm{Re}(K \to (\pi\pi)_{I=2})} = 22.2 \pm 0.1, \qquad (1)$$

with $A_I = a_I \exp(i\delta_I)$ and δ_I the final state interaction phases. This result was particularly enigmatic before the advent of QCD when only the current–current operator Q_2 arising from the W exchange was included in the analysis and, consequently, $\mathrm{Re}a_0/\mathrm{Re}a_2$ was expected to be around one. With the establishment of QCD our understanding of the $\Delta I = 1/2$ selection rule improved considerably. Using the operator product expansion, the $K \to \pi\pi$ amplitudes are obtained from the effective low-energy hamiltonian for $|\Delta S| = 1$ transitions [2–4],

$$\mathcal{H}_{\mathrm{eff}}^{\Delta S=1} = \frac{G_F}{\sqrt{2}} \xi_u \sum_{i=1}^{8} c_i(\mu) Q_i(\mu) \qquad (\mu < m_c), \qquad (2)$$

$$c_i(\mu) = z_i(\mu) + \tau y_i(\mu), \quad \tau = -\xi_t/\xi_u, \quad \xi_q = V_{qs}^* V_{qd}. \qquad (3)$$

The arbitrary renormalization scale μ separates short- and long-distance contributions to the decay amplitudes. The Wilson coefficient functions $c_i(\mu)$ contain all the information on heavy-mass scales. For CP conserving processes only the z_i are numerically relevant. The coefficient functions can be calculated for a scale $\mu \gtrsim 1\,\mathrm{GeV}$ using perturbative renormalization group techniques. They were computed in an extensive next-to-leading logarithm analysis by two groups [5,6]. The local four-quark operators $Q_i(\mu)$ can be written, after Fierz reordering, in terms of color singlet quark bilinears:

$$Q_1 = 4\bar{s}_L \gamma^\mu d_L \bar{u}_L \gamma_\mu u_L, \quad Q_2 = 4\bar{s}_L \gamma^\mu u_L \bar{u}_L \gamma_\mu d_L, \qquad (4)$$

$$Q_3 = 4 \sum_q \bar{s}_L \gamma^\mu d_L \bar{q}_L \gamma_\mu q_L,$$

$$Q_4 = 4\sum_q \bar{s}_{\rm L}\gamma^\mu q_{\rm L}\bar{q}_{\rm L}\gamma_\mu d_{\rm L}, \tag{5}$$

$$Q_5 = 4\sum_q \bar{s}_{\rm L}\gamma^\mu d_{\rm L}\bar{q}_{\rm R}\gamma_\mu q_{\rm R}, \quad Q_6 = -8\sum_q \bar{s}_{\rm L} q_{\rm R}\bar{q}_{\rm R} d_{\rm L}, \tag{6}$$

$$Q_7 = 4\sum_q \frac{3}{2}e_q \bar{s}_{\rm L}\gamma^\mu d_{\rm L}\bar{q}_{\rm R}\gamma_\mu q_{\rm R},$$

$$Q_8 = -8\sum_q \frac{3}{2}e_q \bar{s}_{\rm L} q_{\rm R}\bar{q}_{\rm R} d_{\rm L}, \tag{7}$$

where the sum goes over the light flavors ($q = u, d, s$) and

$$q_{\rm R,L} = \frac{1}{2}(1 \pm \gamma_5)q, \quad e_q = (2/3, -1/3, -1/3). \tag{8}$$

$Q_3, \ldots, Q_6$ arise from QCD penguin diagrams involving a virtual W and a c or t quark, with gluons connecting the virtual heavy quark to the light quarks. They transform as $(8_{\rm L}, 1_{\rm R})$ under $SU(3)_{\rm L} \times SU(3)_{\rm R}$ and solely contribute to $\Delta I = 1/2$ transitions. Q_7 and Q_8 are electroweak penguin operators [7,8] which are less important for the $\Delta I = 1/2$ rule. Long-distance contributions to the amplitudes A_I are contained in the hadronic matrix elements of the four-quark operators,

$$\langle Q_i(\mu)\rangle_I \equiv \langle \pi\pi, I|Q_i(\mu)|K^0\rangle, \tag{9}$$

which are related to the $\pi^+\pi^-$ and $\pi^0\pi^0$ final states through the isospin decomposition

$$\langle Q_i\rangle_0 = \frac{1}{\sqrt{6}}\left(2\langle\pi^+\pi^-|Q_i|K^0\rangle + \langle\pi^0\pi^0|Q_i|K^0\rangle\right), \tag{10}$$

$$\langle Q_i\rangle_2 = \frac{1}{\sqrt{3}}\left(\langle\pi^+\pi^-|Q_i|K^0\rangle - \langle\pi^0\pi^0|Q_i|K^0\rangle\right) = \sqrt{\frac{2}{3}}\langle\pi^+\pi^0|Q_i|K^+\rangle. \tag{11}$$

They are difficult to calculate but can be estimated using non-perturbative techniques generally for μ around a scale of 1 GeV.

Major progress in the understanding of the $\Delta I = 1/2$ rule was made when it was observed that the short-distance (quark) evolution, which is represented by the Wilson coefficient functions in the effective hamiltonian of (2), leads to both an enhancement of the $I = 0$ and a suppression of the $I = 2$ final state. The *octet enhancement* [2] in the (Q_1, Q_2) sector is dominated by the increase of z_2 when μ evolves from M_W down to $\mu \simeq 1\,\text{GeV}$, whereas the suppression of the $\Delta I = 3/2$ transition results from a partial cancellation between the contributions from the Q_1 and Q_2 operators owing to a destructive Pauli interference in the $K^+ \to \pi^+\pi^0$ amplitude. Another important short-distance enhancement was found to arise in the sector of the QCD penguin operators, in particular for z_6, through the proper inclusion of the threshold effects (and the associated incomplete GIM cancellation above the charm quark mass) [9]. Nevertheless, it was concluded that the perturbative QCD effects are far from sufficient to describe the $\Delta I = 1/2$ rule and QCD dynamics at low energies must be addressed. The long-distance enhancement of the matrix elements of the QCD penguin operators over the matrix elements of Q_1 and Q_2 was first conjectured and estimated in [3] in the vacuum saturation approximation (VSA) [10]. The VSA approach, however, fails completely in explaining the $\Delta I = 1/2$ rule, and a more refined method for the calculation of the hadronic matrix elements is certainly needed.

Due to the non-perturbative nature of the long-distance contribution, a large variety of techniques has been proposed to estimate it (for some recent publications see [11–16]). Among the analytical methods, the $1/N_{\rm c}$ expansion [17] ($N_{\rm c}$ being the number of colors) associated with the effective chiral lagrangian is particularly interesting. In this approach, QCD dynamics at low energies is represented by the 'meson evolution' of the operators, from zero momentum to μ, in terms of the chiral loop corrections to the matrix elements [9,18]. The authors of [18] calculated the loop corrections to the matrix elements of Q_1 and Q_2 and included the gluon penguin operator Q_6 at the tree level, consistent with the $1/N_{\rm c}$ expansion. They obtained an additional enhancement and suppression of the $\Delta I = 1/2$ and $\Delta I = 3/2$ amplitudes, respectively, systematically continuing the octet enhancement in the (Q_1, Q_2) sector to the long-distance domain. Numerically, a_2 was reproduced with an accuracy of 70 to approximately 100%, whereas a_0 [for $\Lambda_{\rm QCD} = 300\,\text{MeV}$ and $m_s(1\,\text{GeV}) = 125$–$175\,\text{MeV}$] was found to be around 65–80% of the measured value, suggesting that the bulk of the physics behind the $\Delta I = 1/2$ rule in kaon decays is now understood. One might note that the agreement with experiment is not improved by including the next-to-leading order values for the z_i [19].

In this article we present a new calculation of the hadronic matrix elements in $K \to \pi\pi$ decays in the $1/N_{\rm c}$ expansion for pseudoscalar mesons. The paper contains several improvements over the original approach of [18] which are conceptually and numerically important. One improvement concerns the matching of short- and long-distance contributions to the amplitudes, by adopting a modified identification of virtual momenta in the integrals of the chiral loops. To be explicit, we consider the two currents or densities in the chiral representation of the operators to be connected to each other through the exchange of an effective color singlet boson, and identify its momentum with the loop integration variable. The effect of this procedure is to modify the loop integrals, which introduces noticeable effects in the final results. More important, it provides an unambiguous matching of the $1/N_{\rm c}$ expansion in terms of mesons to the QCD expansion in terms of quarks and gluons. The approach followed here leads to an explicit classification of the diagrams into factorizable and non-factorizable ones. Factorizable loop diagrams refer to the strong sector of the theory and give corrections whose scale dependence is absorbed in the renormalization of the chiral effective lagrangian. The non-factorizable loop diagrams have to be matched to the Wilson coefficients and should cancel scale dependences which arise from the

$$\Pi = \begin{pmatrix} \pi^0 + \frac{1}{\sqrt{3}}a\eta + \sqrt{\frac{2}{3}}b\eta' & \sqrt{2}\pi^+ & \sqrt{2}K^+ \\ \sqrt{2}\pi^- & -\pi^0 + \frac{1}{\sqrt{3}}a\eta + \sqrt{\frac{2}{3}}b\eta' & \sqrt{2}K^0 \\ \sqrt{2}K^- & \sqrt{2}\bar{K}^0 & -\frac{2}{\sqrt{3}}b\eta + \sqrt{\frac{2}{3}}a\eta' \end{pmatrix}, \tag{14}$$

short-distance expansion. In a recent publication together with Bardeen and Paschos [20] we used this method to calculate the hadronic matrix elements of Q_6 and Q_8 which dominate the ratio ε'/ε. In this paper we focus on the CP conserving amplitudes which, to a large extent, are governed by the current–current operators Q_1 and Q_2.

In [18] a mass scale replacing the complete dependence of the exact expressions on the meson masses was introduced in the chiral logarithms. Another improvement of this paper is that we investigate the exact expressions for the matrix elements using the matching prescription discussed above, i.e., we evaluate the complete finite terms from the non-factorizable diagrams. Moreover, we calculate the whole of the matrix elements, that is to say, we also take into account the subleading penguin operators. For consistency with [20] we also include the small effects of the singlet η_0. In the numerical analysis we take special care to separate the different contributions. In particular, we discuss the effect of the final state interaction phases which were not taken into account in [18]. Uncertainties arising from the short-distance part of the calculation are estimated by comparing the amplitudes obtained from the LO and the NLO Wilson coefficients, respectively. Finally, we also investigate the size of higher order corrections to the hadronic matrix elements to critically examine the stability of our results within the pseudoscalar approximation.

In the second part of this work we investigate the matrix element of the ($|\Delta S| = 2$) K^0–$\bar{K}^0$ amplitude in the $1/N_\mathrm{c}$ expansion following the same lines of thought. The introduction to this calculation we postpone to the beginning of Sect. 5. Our results for the $K \to \pi\pi$ matrix elements were already discussed in part in [21,22]. For a more detailed presentation of the general method we refer the reader to [20,23].

The paper is organized as follows. In Sect. 2 we review the general framework of the effective low-energy calculation and discuss the matching of short- and long-distance contributions to the decay amplitudes. Then, in Sect. 3 we investigate the $K \to \pi\pi$ matrix elements. We show explicitly that the scale dependence of the factorizable loop diagrams is absorbed in the renormalization of the bare couplings, the meson wave functions and masses. We next calculate the non-factorizable loop corrections in the cut-off regularization scheme. In Sect. 4 we match them to the Wilson coefficients to obtain the isospin amplitudes. In Sect. 5 we extend the analysis to the ($|\Delta S| = 2$) K^0–$\bar{K}^0$ transition. We compute the matrix element and match it to the short-distance coefficient function to determine the $\hat{B}_K$ parameter. In both sections we present our numerical results and compare them with those of the existing analyses. The conclusions can be found in Sect. 6.

2 General framework

Following the lines of [20] we calculate the hadronic matrix elements of the local four-quark operators (with $|\Delta S| = 1$, 2) in the $1/N_\mathrm{c}$ expansion. To this end we start from the chiral effective lagrangian for pseudoscalar mesons which involves an expansion in momenta where terms up to $\mathcal{O}(p^4)$ are included [24]. Keeping only terms of $\mathcal{O}(p^4)$ which contribute to the $K \to \pi\pi$ or the K^0–$\bar{K}^0$ matrix elements and which are leading in N_c it reads:[1]

$$\begin{aligned} \mathcal{L}_\mathrm{eff} = \frac{f^2}{4}\Big(& \langle D_\mu U^\dagger D^\mu U\rangle + \frac{\alpha}{4N_\mathrm{c}}\langle \ln U^\dagger - \ln U\rangle^2 \\ & + r\langle \mathcal{M}U^\dagger + U\mathcal{M}^\dagger\rangle\Big) \\ & + rL_5\langle D_\mu U^\dagger D^\mu U(\mathcal{M}^\dagger U + U^\dagger\mathcal{M})\rangle \\ & + r^2L_8\langle \mathcal{M}^\dagger U\mathcal{M}^\dagger U + \mathcal{M}U^\dagger\mathcal{M}U^\dagger\rangle, \end{aligned} \tag{12}$$

with $D_\mu U = \partial_\mu U - ir_\mu U + iUl_\mu$, $\langle A\rangle$ denoting the trace of A and $\mathcal{M} = \mathrm{diag}(m_u, m_d, m_s)$. l_μ and r_μ are left- and right-handed gauge fields, respectively, f and r are free parameters related to the pion decay constant F_π and to the quark condensate, with $r = -2\langle\bar{q}q\rangle/f^2$. The complex matrix U is a non-linear representation of the pseudoscalar meson nonet:

$$U = \exp\frac{\mathrm{i}}{f}\Pi, \quad \Pi = \pi^a\lambda_a, \quad \langle\lambda_a\lambda_b\rangle = 2\delta_{ab}, \tag{13}$$

where, in terms of the physical states (see (14) on top of the page) with

$$a = \cos\theta - \sqrt{2}\sin\theta, \quad \sqrt{2}b = \sin\theta + \sqrt{2}\cos\theta, \tag{15}$$

The various conventions and definitions we use are in agreement with [20]. In particular, we introduce the singlet η_0 in the same way and with the same value for the $U_A(1)$ symmetry breaking parameter, $\alpha = m_\eta^2 + m_{\eta'}^2 - 2m_K^2 \simeq 0.72\,\mathrm{GeV}^2$, corresponding to the η–η' mixing angle $\theta = -19°$ [25]. The bosonic representation of the quark currents is defined in terms of (functional) derivatives of the chiral action:

$$\begin{aligned} & \bar{q}_{i\mathrm{L}}\gamma^\mu q_{j\mathrm{L}} \\ & \equiv \frac{\delta S}{\delta(l_\mu(x))_{ij}} = -\mathrm{i}\frac{f^2}{2}\big(U^\dagger\partial^\mu U\big)_{ji} + \mathrm{i}rL_5\big(\partial^\mu U^\dagger\mathcal{M} \\ & \quad -\mathcal{M}^\dagger\partial^\mu U + \partial^\mu U^\dagger U\mathcal{M}^\dagger U - U^\dagger\mathcal{M}U^\dagger\partial^\mu U\big)_{ji}, \end{aligned} \tag{16}$$

and the right-handed currents are obtained by parity transformation. Equation (16) allows us to express the

[1] One might note that the mass term $\propto L_8$ contributes only to the matrix elements of Q_6 and Q_8 which were computed in [20]. Here we include it for completeness

current–current operators in terms of the pseudoscalar meson fields.

The $1/N_c$ corrections to the matrix elements $\langle Q_i \rangle_I$ are calculated by chiral loop diagrams in line with [20]. The factorizable contributions, on the one hand, refer to the strong sector of the theory and give corrections whose scale dependence is absorbed in the renormalization of the chiral effective lagrangian. This property is obvious in the case of the (conserved) currents and was demonstrated explicitly in the case of the bosonized densities [20, 23]. Consequently, the factorizable loop corrections can be computed within dimensional regularization. The non-factorizable corrections, on the other hand, are UV divergent and must be matched to the short-distance part. They are regularized by a finite cutoff which is identified with the short-distance renormalization scale [18,19, 26,27]. The definition of the momenta in the loop diagrams which are not momentum translation invariant was discussed in detail in [20]. A consistent matching is obtained by considering the two currents or densities to be connected to each other through the exchange of a color singlet boson and by assigning the same momentum to it at long and short distances [28–31]. The identification of this momentum with the loop integration variable leads to modified integrals in the chiral loop diagrams compared to those of [18,26]. The numerical implications for the isospin amplitudes in $K \to \pi\pi$ decays and the $\hat{B}_K$ parameter will be addressed in Sects. 4 and 5.

In this paper we investigate the hadronic matrix elements at leading and next-to-leading order in the chiral and the $1/N_c$ expansions. In particular, we calculate the $\mathcal{O}(p^2/N_c)$ corrections to the current–current operators – that is to say, the one-loop corrections over the $\mathcal{O}(p^2)$ lagrangian. The matrix elements of the density–density operators Q_6 and Q_8 are taken from [20]. In the numerical analysis of the $\Delta I = 1/2$ rule and the $\hat{B}_K$ parameter we use the leading logarithmic (LO), as well as, the next-to-leading logarithmic (NLO) values [5,6,32,33] for the ($|\Delta S| = 1, 2$) short-distance coefficient functions.[2] In general, the lack of any reference to the renormalization scheme dependence in the effective low-energy calculation prevents a complete matching at the next-to-leading order [34]. Nevertheless, a comparison of the amplitudes obtained from the LO and NLO coefficients is meaningful as regards testing the validity of perturbation theory.

In the following sections we calculate the long-distance $1/N_c$ corrections to the $K \to \pi\pi$ amplitudes and the $\hat{B}_K$ parameter. First, we investigate the factorizable corrections and show their absorption in the low-energy constants. Secondly, we determine the non-factorizable loops within the modified momentum prescription. Finally, we perform a numerical analysis and compare our results with those of the existing studies.

[2] We treat the coefficient functions as leading order in $1/N_c$ since the large logarithms arising from the long renormalization group evolution from (m_t, M_W) to $\mu \simeq \mathcal{O}(1\,\mathrm{GeV})$ compensate for the $1/N_c$ suppression

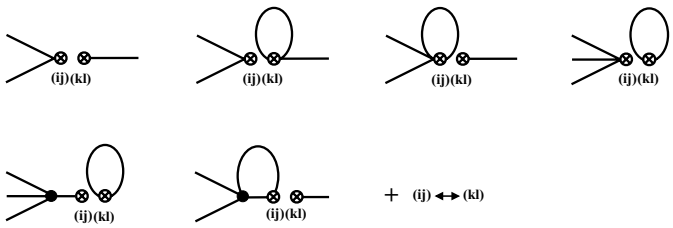

Fig. 1. Factorizable diagrams for the matrix elements of the current–current operators in the isospin limit. Crossed circles represent the bosonized currents, black circles the strong vertices. The lines denote the pseudoscalar mesons. The external legs represent all possible permutations of the kaon and the pions

3 $K \to \pi\pi$ decays

In this section we present the hadronic matrix elements of the current–current operators for the physical decay modes $K^0 \to \pi^+\pi^-$ and $K^0 \to \pi^0\pi^0$ up to $\mathcal{O}(p^4)$ and $\mathcal{O}(p^2/N_c)$ in the parameter expansion. From these results we derive the isospin amplitudes $K \to (\pi\pi)_{I=0,2}$, heading for an explanation of the $\Delta I = 1/2$ selection rule in kaon decays.

3.1 Factorizable $1/N_c$ corrections

The (bare) tree level of the $K \to \pi\pi$ matrix elements, up to $\mathcal{O}(p^4)$ in the chiral expansion, as well as the factorizable $1/N_c$ corrections to the $\mathcal{O}(p^2)$ can be calculated from the tree and loop topologies depicted in Fig. 1. From the sum of these diagrams we obtain[3]

$$\begin{aligned}
&\langle \pi^+\pi^- | Q_2 | K^0 \rangle^F_{(0)} \\
&= \sqrt{2} f \left(m_K^2 - m_\pi^2\right) \left[1 + \frac{4L_5}{f^2}\left(m_K^2 + 4m_\pi^2\right)\right. \\
&\quad \left. - \frac{1}{16\pi^2 f^2}\left(3\lambda_c^2 - \frac{5}{4}\left(m_K^2 + 2m_\pi^2\right)\log\lambda_c^2\right) + \cdots\right], \quad (17)
\end{aligned}$$

where

$$\begin{aligned}
&\langle \pi^+\pi^- | Q_2 | K^0 \rangle^F \\
&= \langle \pi^+\pi^- | Q_4 | K^0 \rangle^F = -\langle \pi^0\pi^0 | Q_1 | K^0 \rangle^F \\
&= \langle \pi^0\pi^0 | Q_4 | K^0 \rangle^F = \frac{2}{3}\langle \pi^0\pi^0 | Q_7 | K^0 \rangle^F, \quad (18)
\end{aligned}$$

and

$$\langle \pi^+\pi^- | Q_i | K^0 \rangle^F = 0 \quad \text{for } i \in \{1,3,5,7\} \quad (19)$$

$$\langle \pi^0\pi^0 | Q_i | K^0 \rangle^F = 0 \quad \text{for } i \in \{2,3,5\}. \quad (20)$$

The ellipses in (17) denote finite terms we omit here for the analysis of the ultraviolet behavior (in particular, they provide the reference scale for the logarithms). We specify

[3] In distinction to [20] the factor i referring to the weak vertex is included in the definition of the matrix element

our results in the cutoff regularization scheme to demonstrate the absorption of the quadratic, as well as the logarithmic divergences as required by current conservation. We note that all factorizable terms quadratic and logarithmic in the cutoff are independent of the momentum prescription in the loop. λ_c is the cutoff for the factorizable diagrams. We introduce two different scales since the factorizable and the non-factorizable corrections refer to disconnected sectors of the theory (strong and weak sectors). Having demonstrated the absence of UV divergent terms in the sum of the factorizable diagrams, in the numerical analysis of the full expressions we will use dimensional regularization, as in pure chiral perturbation theory, which is momentum translation invariant.

If we renormalize the wave functions of the kaon and the pions ($\pi_r \equiv Z_\pi^{1/2}\pi_0$), as well as, the bare decay constant f by using (14)–(17) and (25) of [20], we arrive at the renormalized (factorizable) matrix elements of the ($|\Delta S| = 1$) current–current operators:[4]

$$\langle\pi^+\pi^-|Q_2|K^0\rangle^F_{(r)} = \sqrt{2}F_\pi\left(m_K^2 - m_\pi^2\right)\left[1 + \frac{4\hat{L}_5^r}{F_\pi^2}m_\pi^2\right], \tag{21}$$

where the constant $\hat{L}_5^r$ is defined through the relation [20]

$$\frac{F_K}{F_\pi} \equiv 1 + \frac{4\hat{L}_5^r}{F_\pi^2}(m_K^2 - m_\pi^2), \tag{22}$$

and the remaining matrix elements can be obtained from (18)–(20).

We notice that for the four-quark operators Q_i of the current–current type the divergent terms are absorbed by the renormalization procedure. In addition, the factorizable $1/N_c$ corrections vanish completely, that is to say, the divergent as well as the finite terms. This property has been observed numerically, within dimensional regularization, because the complexity of all factorizable contributions prevents us from doing a fully analytic calculation. Since the factorizable scale λ_c disappears through renormalization, the only matching between long- and short-distance contributions is obtained by identifying the cutoff scale Λ_c of the non-factorizable diagrams with the QCD renormalization scale.

Finally, we note that in the next-to-leading order term of (21) and (22) we used $1/F_\pi$ rather than $1/f$ as was done in [18]. Formally, the difference represents higher order effects. Nevertheless, the appearance of $1/f$ gives rise to a residual dependence on the factorizable scale λ_c, which has no counterpart at the short-distance level and will be absorbed by factorizable loop corrections to the matrix elements at the next order in the parameter expansion. Consequently, it is a more adequate choice to use the physical decay constant in the expressions under consideration. Instead of F_π the kaon decay constant F_K could be used as well. Both choices will be considered in the numerical analysis, which gives a rough estimate of higher order corrections.

[4] The full expressions for the wave function and the decay constants are given in terms of integrals in Appendix A of [20]

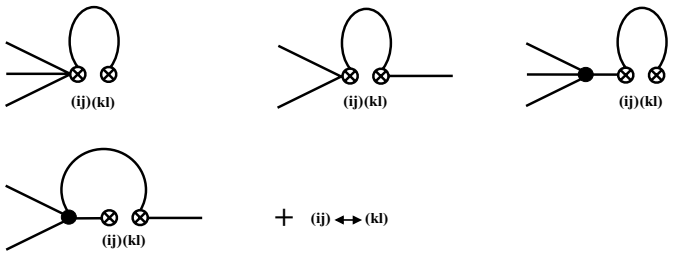

Fig. 2. Non-factorizable diagrams for the matrix elements of the current–current operators in the isospin limit

3.2 Non-factorizable $1/N_c$ corrections

The non-factorizable $1/N_c$ corrections to the hadronic matrix elements constitute the part to be matched to the short-distance Wilson coefficient functions; i.e., the corresponding scale Λ_c has to be identified with the renormalization scale μ of QCD. We perform this identification, as we argued in Sect. 2, by associating the cutoff to the effective color singlet boson. Then, at the $\mathcal{O}(p^2)$ in the chiral expansion, from the diagrams of Fig. 2 we obtain in the SU(2) limit

$$\langle\pi^+\pi^-|Q_1|K^0\rangle^{NF} = -\frac{\sqrt{2}\left(m_K^2 - m_\pi^2\right)}{16\pi^2 F_\pi} \times\left[3\Lambda_c^2 - \left(\frac{1}{4}m_K^2 + 3m_\pi^2\right)\log\Lambda_c^2 + \cdots\right] \tag{23}$$

$$\langle\pi^+\pi^-|Q_2|K^0\rangle^{NF} = \frac{\sqrt{2}\left(m_K^2 - m_\pi^2\right)}{16\pi^2 F_\pi} \times\left[\frac{3}{2}\Lambda_c^2 + \left(m_K^2 - \frac{3}{2}m_\pi^2\right)\log\Lambda_c^2 + \cdots\right] \tag{24}$$

$$\langle\pi^+\pi^-|Q_3|K^0\rangle^{NF} = \frac{\sqrt{2}\left(m_K^2 - m_\pi^2\right)}{16\pi^2 F_\pi}2m_\pi^2\log\Lambda_c^2 + \cdots \tag{25}$$

$$\langle\pi^+\pi^-|Q_4|K^0\rangle^{NF} = \frac{\sqrt{2}\left(m_K^2 - m_\pi^2\right)}{16\pi^2 F_\pi} \times\left[\frac{9}{2}\Lambda_c^2 + \left(\frac{3}{4}m_K^2 - \frac{5}{2}m_\pi^2\right)\log\Lambda_c^2 + \cdots\right] \tag{26}$$

$$\langle\pi^+\pi^-|Q_7|K^0\rangle^{NF} = \frac{\sqrt{2}\left(m_K^2 + 2m_\pi^2\right)}{16\pi^2 F_\pi}\left[\frac{9}{4}\Lambda_c^2 - \frac{1}{8}\left(3m_K^2 + 7m_\pi^2 + \frac{6m_\pi^4}{m_K^2 + 2m_\pi^2}\right)\log\Lambda_c^2 + \cdots\right] \tag{27}$$

$$\langle\pi^0\pi^0|Q_2|K^0\rangle^{NF} = \frac{\sqrt{2}\left(m_K^2 - m_\pi^2\right)}{16\pi^2 F_\pi} \times\left[\frac{9}{2}\Lambda_c^2 + \frac{3}{4}\left(m_K^2 - 6m_\pi^2\right)\log\Lambda_c^2 + \cdots\right] \tag{28}$$

$$\langle\pi^0\pi^0|Q_4|K^0\rangle^{NF} = \frac{\sqrt{2}\left(m_K^2 - m_\pi^2\right)}{16\pi^2 F_\pi} \times\left[\frac{9}{2}\Lambda_c^2 + \frac{1}{4}\left(3m_K^2 - 10m_\pi^2\right)\log\Lambda_c^2 + \cdots\right], \tag{29}$$

where

$$\begin{aligned}&\langle\pi^+\pi^-|Q_3|K^0\rangle^{\mathrm{N}F}\\&\quad=\langle\pi^0\pi^0|Q_3|K^0\rangle^{\mathrm{N}F}=-\langle\pi^0\pi^0|Q_5|K^0\rangle^{\mathrm{N}F}\\&\quad=\frac{1}{2}\langle\pi^0\pi^0|Q_7|K^0\rangle^{\mathrm{N}F}=-\langle\pi^+\pi^-|Q_5|K^0\rangle^{\mathrm{N}F}\end{aligned}\quad(30)$$

and

$$\langle\pi^0\pi^0|Q_1|K^0\rangle^{\mathrm{N}F}=0.\quad(31)$$

One might note that in (23)–(29) [as in (17)] we replaced m_η^2, $m_{\eta'}^2$, and the mixing angle θ by m_π^2 and m_K^2 using the octet–singlet mass matrix of [25].

At this stage of the calculation we find quadratic as well as logarithmic divergences of the non-factorizable corrections. We note that already the leading ($\sim \Lambda_c^2$) terms depend on the momentum prescription. The quadratic terms were calculated in [30] by the background field method. In this paper we investigate the full expressions for the matrix elements needed for the numerical analysis of the amplitudes. The results contain finite terms, originating from the solutions of the integrals listed in (48) and in Appendix B of [20], which we neglect here for brevity and denote by the ellipses. We also note that in the case of Q_7 the solution of the integrals brings about a quartic dependence on the cutoff which has to be cancelled by adding a specific contact interaction proportional to $\delta^{(4)}(0)$ to the Feynman rules of the truncated meson theory [30,35].

Even though the scale dependence of the perturbative coefficient functions is only logarithmic, the full long-distance contribution including the quadratic terms has to be matched to the short-distance part. The quadratic dependence on the cutoff is physical and is necessary for several reasons. First, in the chiral limit ($m_q = 0$) all corrections vanish except for the Λ_c^2 terms, which produce the only scale to be matched to the short distance. Secondly, they stabilize the $1/N_c$ expansion and generally improve the matching of the meson and the quark pictures [18]. Finally, they provide us with a rough estimate of the contributions from higher resonances.

We note that in (23)–(29) we used the physical decay constant F_π rather than f in the same way as for the factorizable diagrams. Again the difference represents higher order effects. However, the (factorizable) scale dependence of f has no counterpart in the short distance and will be absorbed at the next order in the chiral expansion. As for the factorizable contributions the choice of F_K instead of F_π would be also appropriate.

4 Numerical analysis

In this paragraph we list the numerical values for the hadronic matrix elements. We next match them to the Wilson coefficients and study the $K \to (\pi\pi)_{I=0,2}$ isospin amplitudes. In Sect. 4.1 we discuss in detail the $1/N_c$ corrections to the matrix elements. In this context we also calculate the bag parameters, which quantify the deviations from the results obtained in the vacuum saturation approximation and, therefore, are convenient for a comparison with other works. The main results of the present analysis can be found in Sect. 4.2. Therein we give the amplitudes a_0 and a_2 as functions of the matching scale and compare them with the data.

4.1 Hadronic matrix elements

Throughout the numerical analysis we use the following values for the parameters [36]:

$$\begin{aligned}m_\pi &\equiv \big(m_{\pi^0}+m_{\pi^+}\big)/2 = 137.3\,\mathrm{MeV},\\F_\pi &= 92.4\,\mathrm{MeV},\\m_K &\equiv \big(m_{K^0}+m_{K^+}\big)/2 = 495.7\,\mathrm{MeV},\\F_K &= 113\,\mathrm{MeV},\\m_\eta &= 547.5\,\mathrm{MeV},\quad \theta = -19^\circ,\\m_{\eta'} &= 957.8\,\mathrm{MeV},\quad G_F = 1.1664\cdot 10^{-5}\,\mathrm{GeV}^{-2},\\|V_{ud}| &= 0.974,\quad |V_{us}| = 0.22.\end{aligned}$$

Substituting them in (22) we compute $\hat{L}_5^r = 2.07\times 10^{-3}$.

We parameterize our results in terms of the non-perturbative bag parameters $B_i^{(1/2)}$ and $B_i^{(3/2)}$, which quantify the deviations from the values obtained in the vacuum saturation approximation [10]:

$$B_i^{(1/2)} = \frac{\mathrm{Re}\langle Q_i\rangle_0}{\langle Q_i\rangle_0^{\mathrm{VSA}}},\quad i\in\{1,\ldots,8\},\quad(32)$$

$$B_i^{(3/2)} = \frac{\mathrm{Re}\langle Q_i\rangle_2}{\langle Q_i\rangle_2^{\mathrm{VSA}}},\quad i\in\{1,2,7,8\},\quad(33)$$

with $\langle Q_i\rangle_I$ containing both factorizable and non-factorizable contributions. The VSA expressions for the matrix elements are taken from (XIX.11)–(XIX.28) of [19].[5] The numerical values for the matrix elements of the current–current operators are given in Tables 1 and 2. $\langle Q_5\rangle_0^{\mathrm{VSA}}$ and $\langle Q_7\rangle_{0,2}^{\mathrm{VSA}}$ are functions of $R \equiv 2m_K^2/(m_s+m_d) \simeq 2m_K^2/m_s$ and, consequently, depend on the renormalization scale. For comparison, in the tables we also show the results obtained in the large-N_c limit, see (18)–(21). One might note that the different values generally do not coincide, even if the small $\mathcal{O}(p^4)$ term proportional to m_π^2 in (21) [which contributes only at the level of 2% of the $\mathcal{O}(p^2)$ tree level term] is neglected, since in the vacuum saturation approximation Fierz terms are taken into account which are subleading in N_c. In particular, the matrix element $\langle Q_1\rangle_0^{\mathrm{VSA}}$ differs by a factor of $(1-2/N_c)$ from the result obtained at the $\mathcal{O}(p^2)$ in the large-N_c limit. We notice that the inclusion in part of the $1/N_c$ corrections in the VSA method leads to a suppression and enhancement of the $I=0$ and $I=2$ amplitudes, respectively, in complete disagreement with the data.

In Tables 3 and 4 we list our results for the hadronic matrix elements at next-to-leading order in the chiral and

[5] Note that our definition of the pion decay constant ($F_\pi = 92.4\,\mathrm{MeV}$) differs by a factor of $1/2^{1/2}$ from the one used in [19]

Table 1. $I = 0$ matrix elements of the current–current operators: VSA vs. tree level (large-N_c limit), in units of $10^6 \cdot \mathrm{MeV}^3$ (R in units of GeV)

	$\langle Q_1\rangle_0$	$\langle Q_2\rangle_0$	$\langle Q_3\rangle_0$	$\langle Q_4\rangle_0$	$\langle Q_5\rangle_0$	$\langle Q_7\rangle_0$
VSA	-4.03	20.2	12.1	36.3	$-11.7 \cdot R^2$	$18.2 + 32.5 \cdot R^2$
tree	-12.3	24.6	0	37.0	0	18.5

Table 2. Same as in Table 1, now for the $I = 2$ matrix elements

	$\langle Q_1\rangle_2$	$\langle Q_2\rangle_2$	$\langle Q_7\rangle_2$
VSA	22.8	22.8	$-25.7 + 18.9 \cdot R^2$
tree	17.4	17.4	-26.1

the $1/N_c$ expansions. The matrix elements of the current–current operators are calculated from (18)–(31) including the finite terms denoted by the ellipses. The results for the operators Q_6 and Q_8 are taken from [20]. These results contain the leading plus next-to-leading order terms in the chiral expansion of the density–density operators as well as the leading $1/N_c$ corrections, that is to say, the $\mathcal{O}(p^0)$, $\mathcal{O}(p^2)$, and $\mathcal{O}(p^0/N_c)$. Note that the matrix elements generally contain a non-vanishing imaginary part (scale independent at the one-loop level) which is due to on-shell (π–π) rescattering effects.

The isospin amplitudes are largely dominated by the operators Q_1 and Q_2. Therefore it is instructive to analyze in detail the $1/N_c$ corrections to these two operators. To this end we next give the analytic expressions for the isospin matrix elements of Q_1 and Q_2:

$$\begin{aligned}\langle Q_1\rangle_0 = &-\frac{1}{\sqrt{3}}F_\pi\left(m_K^2 - m_\pi^2\right)\left[1 + \frac{4\hat{L}_5^r}{F_\pi^2}m_\pi^2 + \frac{1}{(4\pi)^2F_\pi^2}\right.\\ &\left.\times\left(6\Lambda_c^2 - \left(\frac{1}{2}m_K^2 + 6m_\pi^2\right)\log\left(1 + \frac{\Lambda_c^2}{\tilde{m}^2}\right)\right)\right]\\ &+a_{10}[\tilde{m}], \qquad (34)\\ \langle Q_2\rangle_0 = &\frac{2}{\sqrt{3}}F_\pi\left(m_K^2 - m_\pi^2\right)\left[1 + \frac{4\hat{L}_5^r}{F_\pi^2}m_\pi^2 + \frac{1}{(4\pi)^2F_\pi^2}\right.\\ &\left.\times\left(\frac{15}{4}\Lambda_c^2 + \left(\frac{11}{8}m_K^2 - \frac{15}{4}m_\pi^2\right)\log\left(1 + \frac{\Lambda_c^2}{\tilde{m}^2}\right)\right)\right]\\ &+a_{20}[\tilde{m}], \qquad (35)\\ \langle Q_1\rangle_2 = &\langle Q_2\rangle_2\\ = &\sqrt{\frac{2}{3}}F_\pi\left(m_K^2 - m_\pi^2\right)\left[1 + \frac{4\hat{L}_5^r}{F_\pi^2}m_\pi^2 + \frac{1}{(4\pi)^2F_\pi^2}\right.\\ &\left.\times\left(-3\Lambda_c^2 + \left(\frac{1}{4}m_K^2 + 3m_\pi^2\right)\log\left(1 + \frac{\Lambda_c^2}{\tilde{m}^2}\right)\right)\right]\\ &+a_{21}[\tilde{m}]. \qquad (36)\end{aligned}$$

Equations (34)–(36) allow us to compare our results with the analytic expressions of [18]. First, we note that the modified matching which was discussed in Sect. 2 increases the terms quadratic in the cutoff by a factor of 3/2 relative to the results presented therein. This was already observed in [30]. The modification of the quadratic terms provides an additional octet enhancement in the long-distance domain. The logarithmic terms, on the other hand, are modified only on account of the presence of the η_0. To be explicit, in the octet limit [i.e., in the absence of the η_0, with $a = b = 1$ and $m_\eta^2 = (4m_K^2 - m_\pi^2)/3$] the coefficient of the logarithm in (34) is reduced to $(m_K^2/2 + 10m_\pi^2/3)$ whereas the other terms remain unchanged. The separation of the logarithmic and the finite terms in (34)–(36) is arbitrary and is done, for comparison with [18], by introducing a mass scale replacing the dependence of the exact expressions on the meson masses in the chiral logarithms. The logarithmic and the finite terms (a_{iI}) defined in this way each depend on the choice of the mass scale $\tilde{m}$, whereas the sum of all contributions is independent of this parameter. We calculated the complete finite terms arising from the non-factorizable loop diagrams using the matching prescription advocated in [20,30].[6] These terms were not included in [18]. Consequently, the numerical values of the matrix elements reported therein exhibit a dependence on the specific choice of the mass scale in the logarithms which is absent in the present calculation.

In Table 5 we split up the numerical values for the $I = 0$ and $I = 2$ matrix elements of Q_1 and Q_2 with respect to the quadratic, the logarithmic, and the finite terms, respectively, at a cutoff scale of $\Lambda_c = 800\,\mathrm{MeV}$. From the table we see that the finite terms are of the same order of magnitude as the logarithmic ones and, therefore, must be considered at the same level in the numerical analysis. These terms are generally suppressed by a factor of $\delta \equiv m_{K,\pi}^2/(4\pi F_\pi)^2 < 20\%$ with respect to the leading $\mathcal{O}(p^2)$ tree level. In addition, as can be seen from (34)–(36) and Table 5, no coefficient larger than one or two which could significantly enhance them has been found. This is different from the quadratic terms which are not suppressed as their relative size is determined by $\Delta \equiv \Lambda_c^2/(4\pi F_\pi)^2$ and, moreover, they appear with larger prefactors [even as large as six in (34)].[7] Consequently, in the case of the $I = 0$ matrix elements of Q_1 and Q_2

[6] For details on the computation of the loop integrals see Appendix B of [20]

[7] It is interesting to note that the non-suppression of the quadratic terms presumably could be important for Q_6 but less important for Q_8. On the one hand, the first non-vanishing tree level contribution to the operators Q_6 and Q_8 is of the $\mathcal{O}(p^2)$ and $\mathcal{O}(p^0)$, respectively. On the other hand, the first non-vanishing quadratic corrections to both operators are of the $\mathcal{O}(p^2/N_c)$ (terms of the $\mathcal{O}(p^0/N_c)$ were found to be only logarithmic [20]). Consequently, in the case of Q_8 the quadratic terms are (chirally) suppressed by a factor of $p^2 \cdot \Delta$ with respect to the (leading) tree level contribution whereas in the case of Q_6 they bring about only a factor of Δ. Quadratic terms, even though subleading in N_c, could therefore significantly affect the matrix element of Q_6 especially if large prefactors are observed as for Q_1 and Q_2 in (34)–(36). This difference between the Q_6 and Q_8 operators could play an important role for ε'/ε. This point will be investigated in [37]

Table 3. Hadronic matrix elements of $Q_{1,\ldots,5,7}$ (in units of $10^6 \cdot \mathrm{MeV}^3$) and $Q_{6,8}$ (in units of $R^2 \cdot \mathrm{MeV}$) in the isospin limit for the $I = 0$ amplitudes, shown for various values of the cutoff Λ_c

Λ_c	0.5 GeV	0.6 GeV	0.7 GeV	0.8 GeV	0.9 GeV	1.0 GeV	
$\langle Q_1\rangle_0$	−27.4	−33.2	−40.2	−48.2	−57.3	−67.4	−5.55i
$\langle Q_2\rangle_0$	50.0	58.8	68.8	79.9	92.4	106	11.1i
$\langle Q_3\rangle_0$	0.04	0.05	0.03	−0.02	−0.12	−0.26	0
$\langle Q_4\rangle_0$	77.5	92.1	109	128	150	173	16.6i
$\langle Q_5\rangle_0$	−0.04	−0.05	−0.03	0.02	0.12	0.26	0
$\langle Q_6\rangle_0$	−44.1	−38.6	−33.7	−29.4	−25.5	−21.9	0
$\langle Q_7\rangle_0$	34.4	40.1	46.6	54.1	62.6	72.2	8.32i
$\langle Q_8\rangle_0$	118	119	119	119	118	117	36.7i

Table 4. Same as in Table 3, now for the $I = 2$ amplitudes

Λ_c	0.5 GeV	0.6 GeV	0.7 GeV	0.8 GeV	0.9 GeV	1.0 GeV	
$\langle Q_1\rangle_2$	6.54	2.51	−2.26	−7.77	−14.0	−21.1	−3.45i
$\langle Q_2\rangle_2$	6.54	2.51	−2.26	−7.77	−14.0	−21.1	−3.45i
$\langle Q_7\rangle_2$	−14.5	−10.7	−6.27	−1.15	4.67	11.2	5.18i
$\langle Q_8\rangle_2$	39.9	35.3	31.2	27.2	23.2	18.8	−11.5i

Table 5. Different contributions to the hadronic matrix elements of Q_1 and Q_2 (in units of $10^6 \cdot \mathrm{MeV}^3$) for $\Lambda_c = 800\,\mathrm{MeV}$ and $\tilde{m} = 300\,\mathrm{MeV}$

	$\langle Q_1\rangle_0$	$\langle Q_1\rangle_2$	$\langle Q_2\rangle_0$	$\langle Q_2\rangle_2$
tree	−12.3	17.4	24.6	17.4
Λ_c^2	−34.5	−24.4	43.1	−24.4
$\log \Lambda_c[\tilde{m}]$	4.43	3.13	10.0	3.13
finite	−5.83 − 5.55i	−3.90 − 3.45i	2.20 + 11.1i	−3.90 − 3.45i
total	−48.2 − 5.55i	−7.77 − 3.45i	79.9 + 11.1i	−7.77 − 3.45i

both the logarithmic and the finite corrections are moderate, and the chiral limit gives a satisfactory representation of the full amplitude provided that the matching scale is taken sufficiently large ($\Lambda_c \gtrsim$ 500–600 MeV). In the case of the $I = 2$ matrix elements we also observe that the quadratic terms are enhanced with respect to the tree level, whereas the logarithmic and the finite terms are largely suppressed. However, in this case the quadratic corrections counteract the tree level, and the sum of both contributions is no longer large compared to the logarithmic and the finite terms. Therefore the neglect of either of the terms is no longer justified. In particular, we observe that for the $\Delta I = 3/2$ channel the chiral limit gives a better approximation to the exact result than a calculation which includes only the logarithms without taking into account the finite terms. This remark also holds for the matrix element $\langle Q_1\rangle_0$. Finally, we note that variation of the mass scale in the logarithms $[m_\pi < \tilde{m} < m_K]$ in [18] has a noticeable effect on the numerical value of the $I = 2$ amplitude.

When comparing the results of the present analysis with those of [18] one has to take into account another difference in the treatment of the next-to-leading order terms: in (34)–(36) we used $1/F_\pi$ rather than the bare parameter $1/f$ as was done in [18]. Formally, the difference concerns higher order effects, as we already discussed above. However, since the factorizable scale which appears in the bare coupling f will be absorbed by factorizable loop corrections to the matrix elements at the next order in the parameter expansion, it has not to be matched to any short-distance contribution. Consequently, it is a more adequate choice to use the physical decay constant in the expressions under consideration. The effect of this different treatment of the next-to-leading order terms will be further discussed in Sect. 4.2.

In Tables 6 and 7 we list the values we compute for the bag parameters $B_i^{(1/2)}$ and $B_i^{(3/2)}$. We find a large enhancement of $B_1^{(1/2)}$ and $B_2^{(1/2)}$ over the VSA result, which constitutes the dominant contribution, at long distances, to the $\Delta I = 1/2$ transition in $K \to \pi\pi$ decays. Moreover,

Table 6. Bag parameters for the $I = 0$ amplitudes, shown for various values of the cutoff. $B_{5,7,8}^{(1/2)}$ depend on $R \simeq 2m_K^2/m_s$ and are calculated for a running $m_s(\mu = \Lambda_c)$ at the leading logarithmic order ($\Lambda_{\rm QCD} = 325\,{\rm MeV}$) with $m_s(1\,{\rm GeV}) = 175\,{\rm MeV}$

Λ_c	0.5 GeV	0.6 GeV	0.7 GeV	0.8 GeV	0.9 GeV	1.0 GeV
$B_1^{(1/2)}$	6.75	8.24	9.98	12.0	14.2	16.6
$B_2^{(1/2)}$	2.47	2.91	3.41	3.96	4.57	5.23
$B_3^{(1/2)}$	0.003	0.004	0.002	−0.002	−0.010	−0.021
$B_4^{(1/2)}$	2.12	2.54	3.00	3.53	4.13	4.75
$B_5^{(1/2)}$	0.0004	0.0009	0.0005	−0.0003	−0.0014	−0.0020
$B_6^{(1/2)}$	1.26	1.10	0.96	0.84	0.72	0.62
$B_7^{(1/2)}$	0.15	0.16	0.18	0.21	0.23	0.26
$B_8^{(1/2)}$	1.20	1.21	1.21	1.21	1.20	1.19

Table 7. Same as in Table 6, now for the $I = 2$ amplitudes.

Λ_c	0.5 GeV	0.6 GeV	0.7 GeV	0.8 GeV	0.9 GeV	1.0 GeV
$B_1^{(3/2)}$	0.29	0.11	−0.10	−0.34	−0.61	−0.92
$B_2^{(3/2)}$	0.29	0.11	−0.10	−0.34	−0.61	−0.92
$B_7^{(3/2)}$	−0.15	−0.10	−0.06	−0.01	0.04	0.09
$B_8^{(3/2)}$	0.72	0.64	0.56	0.49	0.42	0.34

we obtain the correct scale dependence counteracting the scale behavior of the Wilson coefficients z_1 and z_2, which leads to an acceptable matching (see Sect. 4.2). In view of the large corrections one might question the convergence of the $1/N_{\rm c}$ expansion. However, there is no strong reason for such doubts because the non-factorizable contribution we consider in this paper represents the first term in a new type of a series absent in the large-$N_{\rm c}$ limit. It is reasonable to assume that this leading non-factorizable term carries a large fraction of the whole contribution [18] (see also the discussion in Sect. 4.2). $B_3^{(1/2)}$ and $B_5^{(1/2)}$ turn out to be very close to zero. This property is due to the vanishing tree level as well as to the small $1/N_{\rm c}$ corrections proportional to $m_\pi^2/(4\pi F_\pi)^2$, see (25) and (30). We notice that the small contribution of the operator Q_5 to ε'/ε is even further reduced when replacing the VSA expression for $\langle Q_5\rangle_0$, which is commonly used in the analysis of ε'/ε [34], by the result presented in this paper. $B_7^{(1/2)}$ and $B_7^{(3/2)}$ are also found to be significantly reduced with respect to the vacuum saturation approximation. In particular, $B_7^{(3/2)}$ turns out to be negative for small values of the cutoff.[8] We also notice a decrease of the $B_1^{(3/2)}$ and $B_2^{(3/2)}$ parameters, which are relevant for A_2. However, as we will see below, their scale dependence largely overcompensates for the variation of the short-distance coefficient functions. Nevertheless, as the values are found to be reduced, they generally account for the reduction of the $I = 2$ amplitude. Finally, $B_6^{(1/2)}$ receives only small corrections whereas $B_8^{(3/2)}$ turns out to be substantially reduced relative to the VSA result [20]. The numerical implications for ε'/ε will be investigated elsewhere [37]. One might note that the numerical values of $B_8^{(3/2)}$ shown in Table 7 differ from the ones given in Table 2 of [20]. This is due to the fact that in the present paper we include only the real part of the hadronic matrix elements in the definition of the B_i parameters (see Sect. 4.2).

4.2 The $\Delta I = 1/2$ rule

We next investigate the CP conserving amplitudes ${\rm Re}a_0$ and ${\rm Re}a_2$. To this end we start from the expression for the isospin amplitudes A_I which contain the $(\pi$–$\pi)$ strong interaction phase shift for the $I = 0$ and the $I = 2$ final states, respectively,

$$A_{I=0,2} = \frac{G_F}{\sqrt{2}} V_{ud}V_{us}^* \sum_i c_i(\mu)\langle Q_i(\mu)\rangle_{I=0,2}. \qquad (37)$$

Then

$$\begin{aligned} {\rm Re}a_I &= \frac{G_F}{\sqrt{2}} V_{ud}V_{us}^* \Big| \sum_i z_i \langle Q_i\rangle_I \Big| \\ &= \frac{G_F}{\sqrt{2}} V_{ud}V_{us}^* \frac{1}{\cos\delta_I} \sum_i z_i {\rm Re}\langle Q_i\rangle_I. \end{aligned} \qquad (38)$$

Within an exact realization of non-perturbative QCD the two expressions in (38) are equivalent. However, in the approximate low-energy calculation of the present work the long-distance imaginary part which we computed at the one-loop level (see Tables 3 and 4) is not expected to be of the same accuracy as the real part obtained at this level. In particular, as the one-loop (long-distance) imaginary part is scale independent, it cannot compensate for the scale dependence of the Wilson coefficients z_i leading to a scale dependent imaginary part of the total amplitude. This requires a calculation of the (long-distance) imaginary part at least at the two-loop level which will introduce a scale dependence. In addition, the two-loop contribution is expected to be of the same order of magnitude as the one-loop contribution which only appears at the level of the finite terms, as it will bring about a quadratically divergent term. This situation is analogous to the non-suppression of the one-loop contribution to the real part ($\sim \Delta$) with respect to the tree level. The two-loop contribution to the real part, on the other hand, is expected to be suppressed by at least a factor of δ with respect to the tree level and

[8] Very recently [38] the first non-trivial $1/N_{\rm c}$ corrections to the matrix elements of Q_7 were evaluated using the methods of [39]. The numerical results were also sensitive to the choice of the renormalization scale. In particular, negative values for $B_7^{(1/2)}$ and $B_7^{(3/2)}$ were found below $\mu \lesssim 1.3\,{\rm GeV}$, in qualitative agreement with the results of the present analysis but in disagreement with the large positive values obtained in the chiral quark model at a matching scale of 0.8 GeV [40]

Table 8. Rea_0 and Rea_2 (in units of 10^{-4} MeV) for $m_s(1\,\mathrm{GeV}) = 175\,\mathrm{MeV}$, $\Lambda_{\overline{\mathrm{MS}}}^{(4)} = 325\,\mathrm{MeV}$, and various values of the matching scale $\mu = \Lambda_c$

	Rea_0			Rea_2		
Λ_c	LO	NDR	HV	LO	NDR	HV
0.5 GeV	3.90	0.74	4.48	0.063	0.086	0.063
0.6 GeV	3.50	2.58	3.57	0.027	0.032	0.028
0.7 GeV	3.53	2.89	3.45	−0.025	−0.028	−0.025
0.8 GeV	3.75	3.13	3.58	−0.090	−0.101	−0.095
0.9 GeV	4.08	3.42	3.83	−0.167	−0.188	−0.178
1.0 GeV	4.49	3.76	4.17	−0.257	−0.289	−0.274
exp.		3.33			0.15	

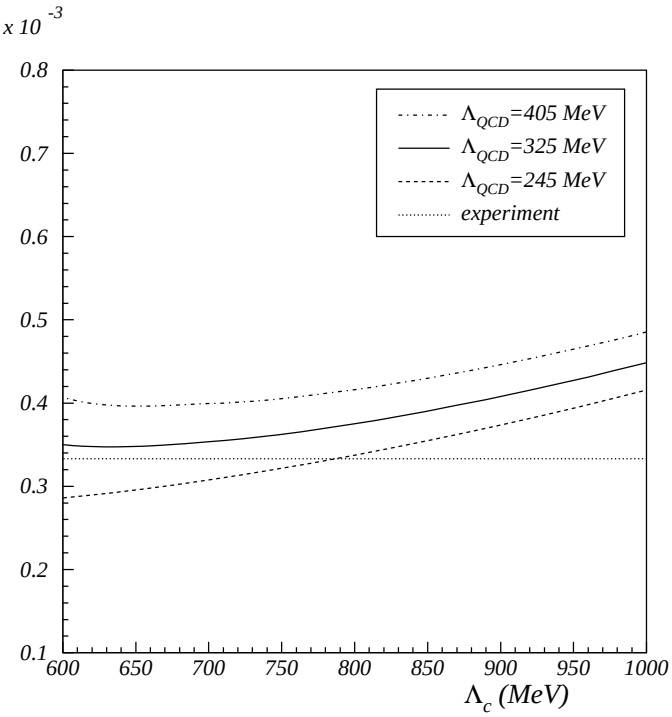

Fig. 3. Rea_0 (in units of MeV) with LO z_i for $m_s(1\,\mathrm{GeV}) = 175\,\mathrm{MeV}$ and various values of Λ_{QCD} as a function of the matching scale $\Lambda_c = \mu$

the one-loop contribution. This is analogous to the one-loop logarithmic and finite terms which are suppressed by a factor of δ with respect to the tree level. For the numerical analysis we will therefore consider only the real part of the matrix elements [see the second expression in (38)] using the experimental values of the final state interaction phases, $\delta_0^{\mathrm{exp}} = (37 \pm 3)^\circ$ and $\delta_2^{\mathrm{exp}} = (-7 \pm 1)^\circ$ [41]. This procedure has also been followed in [42]. However, as the imaginary part is a loop effect (suppressed by a factor of δ with respect to the tree level contribution), its effect on the absolute value of the amplitude strictly speaking is of the two-loop order. Consequently, we will also compare our results with the ones obtained by taking the (long-distance) imaginary part to zero, i.e., by taking $\sum_i z_i \langle Q_i \rangle_I = \sum_i z_i \mathrm{Re}\langle Q_i \rangle_I$. This holds for an estimate of the size of higher order effects which is generally disregarded in the literature.

In Table 8 we show the numerical values of the amplitudes for various values of the matching scale and fixed values of $\Lambda_{\mathrm{QCD}} = \Lambda_{\overline{\mathrm{MS}}}^{(4)}$ and the strange quark mass m_s. The numerical analysis is done using the leading logarithmic as well as the next-to-leading logarithmic values of the Wilson coefficients listed in the Appendix. The NLO values are scheme dependent and are calculated within naive dimensional regularization (NDR) and in the 't Hooft–Veltman scheme (HV), respectively.[9] The difference between the two NLO results at a given scale reveals the uncertainty due to the lack of any reference to the renormalization scheme dependence in the effective low-energy calculation.

In Fig. 3 we show Rea_0 calculated with leading order Wilson coefficients for various values of Λ_{QCD} as a function of the matching scale. We take the (conservative) range of $\Lambda_{\mathrm{QCD}} = 325 \pm 80\,\mathrm{MeV}$ which corresponds to $\alpha_s(M_Z) = 0.118 \pm 0.005$ [34]. First, we note that our result for a_0 shows an additional enhancement (around 30–50% of the experimental value) compared to the result of [18] which renders the amplitude in good agreement with the observed value for low values of the scale or even larger than the experimental value for large values of the scale. A significant enhancement arises from the Q_1 and Q_2 operators due to the modified matching prescription in the non-factorizable sector we discussed above. Numerically, at a scale of $\Lambda_c = 800\,\mathrm{MeV}$ the modified momentum routing accounts for approximately 20% of the final number(s) presented in Fig. 3. Another enhancement with respect to [18] originates from the correction of the real part by the experimental phase [see (38)]. Neglecting completely the effect of the (π–π) phase shift would reduce our result by a factor of $\cos\delta_0 \simeq 0.8$. The remainder is due to the choice of the physical value F_π instead of f in the next-to-leading order terms of the factorizable and non-factorizable corrections. Our result depends only moderately on the matching scale although the stability falls off for large values of the scale around 1 GeV. We observe a cancellation between the scale dependence of the short- and long-distance contributions, i.e., the operator evolution in the quark picture is continued with the same pattern in the meson picture. The main uncertainty displayed in Fig. 3 originates from the dependence of the Wilson coefficients on Λ_{QCD}. The uncertainty increases for very low values of the scale reflecting the poor perturbative behavior expected at those scales especially for the large value of $\Lambda_{\mathrm{QCD}} = 405\,\mathrm{MeV}$. Within the (conservative) range of $\Lambda_{\mathrm{QCD}} = 325 \pm 80\,\mathrm{MeV}$ we considered, the value 405 MeV leads to the most distinct deviation from the experimental result which, however, does not exceed approximately 20% of the observed value in the range $600\,\mathrm{MeV} \lesssim \Lambda_c \lesssim 800\,\mathrm{MeV}$ where the minimum occurs and the dependence on the scale is weak.

[9] We are very thankful to M. Jamin for providing us with the numerical values of the Wilson coefficients used in this section

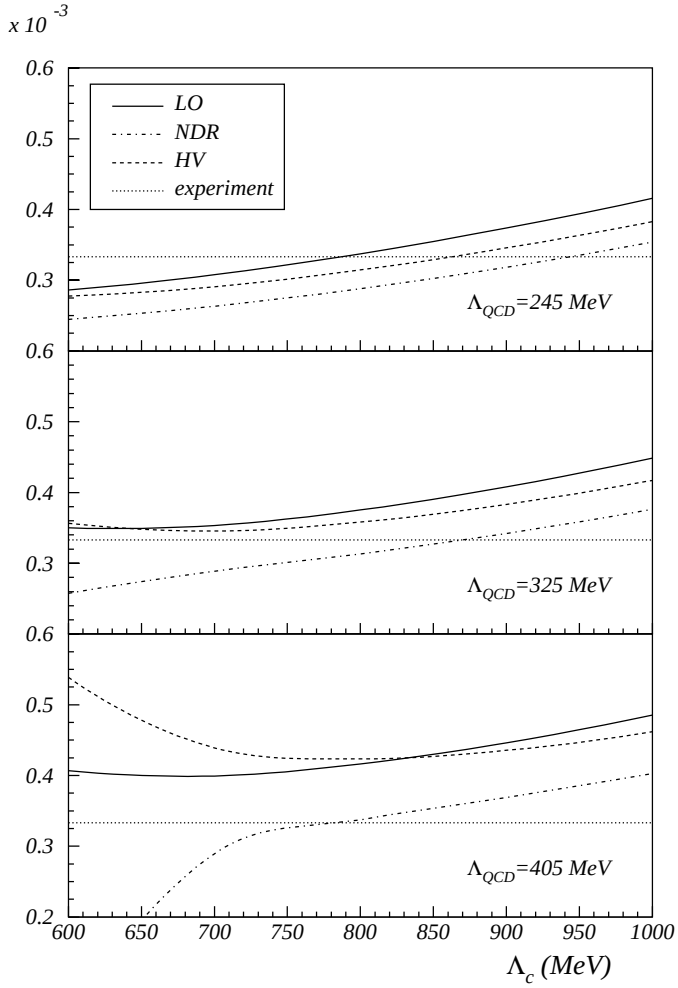

Fig. 4. Rea_0 (in units of MeV) with LO and NLO z_i for $m_s(1\,\mathrm{GeV}) = 175\,\mathrm{MeV}$ and various values of Λ_{QCD} as a function of the matching scale $\Lambda_c = \mu$

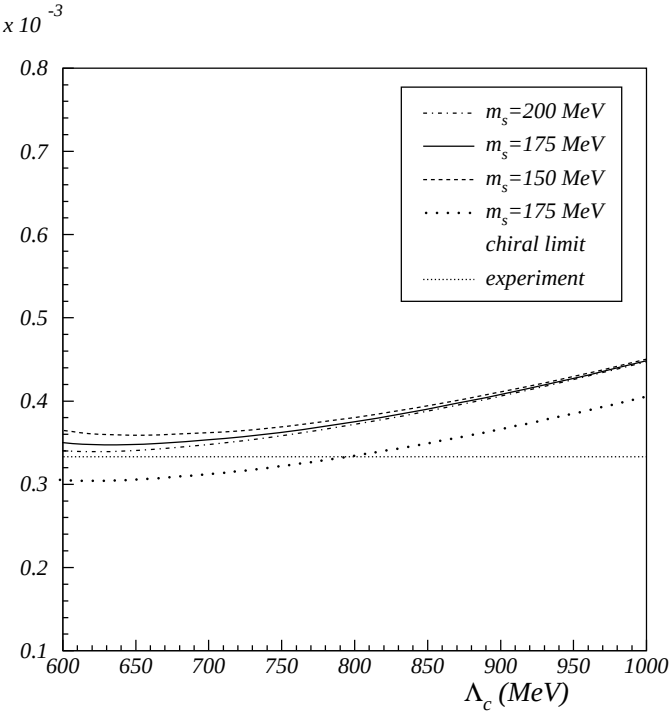

Fig. 5. Rea_0 (in units of MeV) with LO z_i for $\Lambda_{\mathrm{QCD}} = 325\,\mathrm{MeV}$ and various values of $m_s(1\,\mathrm{GeV})$ as a function of the matching scale $\Lambda_c = \mu$

In Fig. 4 we compare the results for Rea_0 we obtain using the LO and NLO Wilson coefficients, respectively. In the HV scheme, for moderate values of Λ_{QCD} introducing the NLO coefficients does not significantly affect the numerical values of the $\Delta I = 1/2$ amplitude which is found to be only slightly suppressed with respect to the LO result. The main effect of the NLO coefficients is that they further reduce the dependence on the matching scale. This statement does not hold within the NDR scheme. In this scheme, for $\Lambda_{\mathrm{QCD}} = 245\,\mathrm{MeV}$ the effect of the NLO coefficients is also moderate but noticeably increases for large values of Λ_{QCD} leading to a distinct suppression of the LO result. For values of Λ_{QCD} as large as 405 MeV both the HV and the NDR results rapidly diverge for low values of the matching scale ($\lesssim 700\,\mathrm{MeV}$) indicating the loss of perturbativity. Taking into account the fact that we do not incorporate the effects of higher resonances and cannot adopt too high values of the scale, a choice of Λ_c around 700–800 MeV seems to be most appropriate. For $\Lambda_{\mathrm{QCD}} = 325\,\mathrm{MeV}$ (245 MeV) the effect of the NLO coefficients is less pronounced, and scales as low as 600–650 MeV (500 MeV), where the LO minimum occurs, appear to be acceptable. Above these scales the deviation of the NLO results from the experiment does not exceed 20–25% of the experimental value. Moreover, the difference between LO and NLO (HV and NDR) values is moderate, of the order of at most 20–25% of the observed value.[10] In all the cases the tendency for a large enhancement of the required size remains present.

In Fig. 5 we show the weak dependence of Rea_0 (with LO Wilson coefficients) on the strange quark mass which arises from the matrix element of the gluon penguin operator $[\langle Q_6\rangle_0 \propto 1/m_s^2]$. We notice that the contribution from Q_6 to the $\Delta I = 1/2$ amplitude for small values of the cutoff ($\sim 600\,\mathrm{MeV}$) roughly varies between 10–20% of the total value and significantly decreases for large values of Λ_c. This behavior is also found when the NLO coefficients are used. The effect of the remaining (penguin) operators is very small (below 1% of the total result except for Q_4 which contributes at the level of -3%). For comparison, in Fig. 5 we also show Rea_0 calculated in the chiral limit. We observe that the result obtained in the chiral limit, for reasons explained above, is rather close to the numerically exact one, that is to say, the logarithmic and the finite terms in the non-factorizable corrections to the matrix elements are of minor importance provided that the matching scale is taken sufficiently large ($\Lambda_c \gtrsim 500$–$600\,\mathrm{MeV}$). Finally, we note that the presence of the η_0

[10] The comparison of the LO and NLO coefficients should be used with caution as it partly originates from a change in the value of the QCD coupling for a chosen value of $\Lambda_{\overline{\mathrm{MS}}}$ [19]

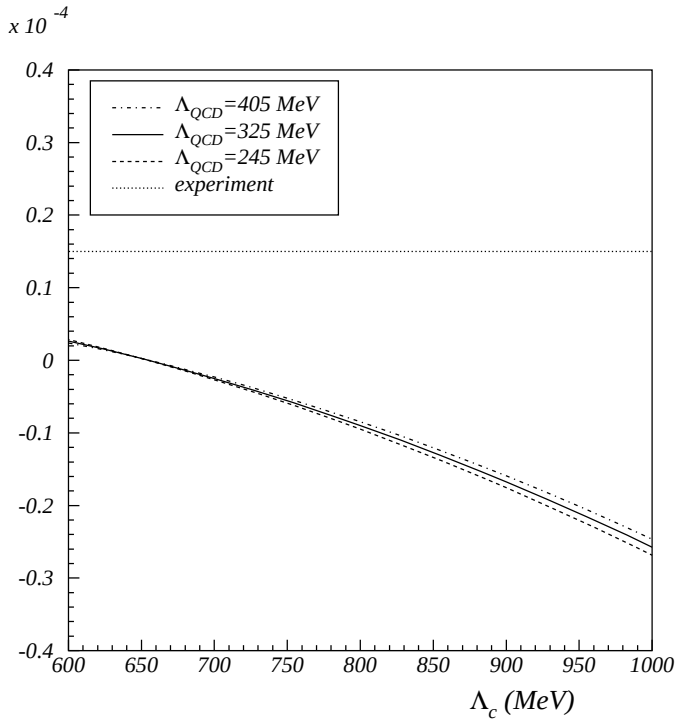

Fig. 6. Rea_2 (in units of MeV) with LO z_i for various values of $\Lambda_{\rm QCD}$ as a function of the matching scale $\Lambda_c = \mu$

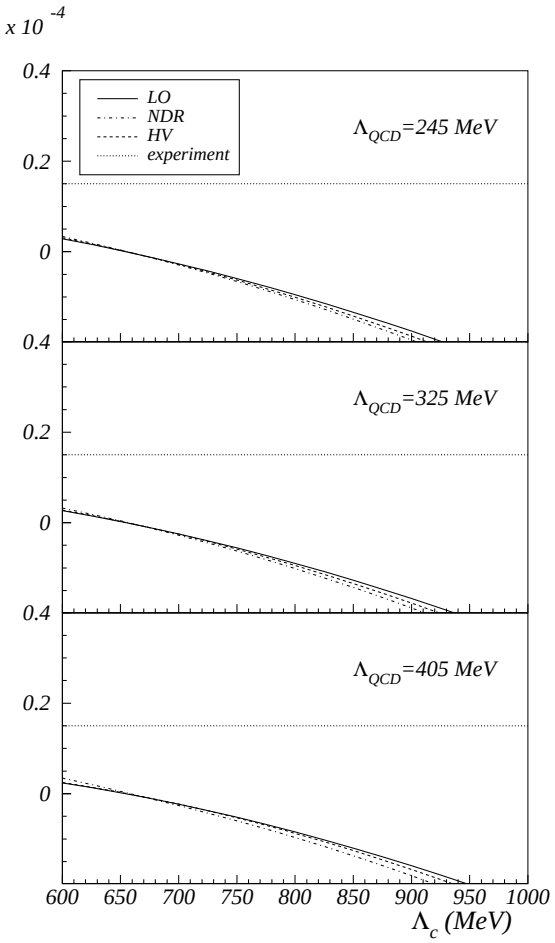

Fig. 7. Rea_2 (in units of MeV) with LO and NLO z_i for various values of $\Lambda_{\rm QCD}$ as a function of the matching scale $\Lambda_c = \mu$

does not affect the numerical values of the amplitudes (in the octet limit the numbers given in Table 8 change by less than 1%).

In distinction to the $\Delta I = 1/2$ amplitude, the $\Delta I = 3/2$ amplitude depicted in Fig. 6 (with LO Wilson coefficients) is highly unstable. In addition, the numerical values lie well below the measured value. The amplitude even changes sign [due to the large negative coefficient of the quadratic term in (36)]. The large uncertainty can be understood, as we already discussed above, from the fact that the two numerically leading terms, the tree level and the one-loop quadratically divergent term, have approximately the same size but opposite sign. On the one hand, this property is generally welcomed as it explains the origin of the suppression of the $\Delta I = 3/2$ amplitude which turns out to be sufficiently suppressed whatever the particular chosen scale is between 600 MeV and 900 MeV. On the other hand, the large cancellation implies that the result will be significantly affected by higher order terms which are expected to be of the order of the one-loop logarithmic and finite terms. We note that the agreement with the experimental value is not improved in the chiral limit. We also notice that the numerical values depicted in Fig. 6 depend only weakly on the choice of $\Lambda_{\rm QCD}$. In Fig. 7 we compare the results for Rea_2 we obtain using the LO and NLO Wilson coefficients, respectively. We observe that the effect of the NLO coefficients is negligible with respect to the large discrepancy between our results and the observed value. The small effect of the NLO coefficients indicates the validity of perturbation theory and further supports the supposition that the discrepancy is due the lack of accuracy in the low-energy part of the calculation.

The typical size of higher order effects in the calculation of the hadronic matrix elements can be estimated in various ways. First, as we already mentioned above, one may replace in all NLO terms the coefficient $1/F_\pi$ by $1/F_K$. The results obtained in this case [denoted by (b)] are shown in Figs. 8 and 9. The $\Delta I = 1/2$ amplitude is suppressed by approximately 20% with respect to the result we obtained using $1/F_\pi$ [denoted by (a)] and is even in better agreement with the observed value. The $\Delta I = 3/2$ amplitude, on the other hand, is enhanced but still far too much suppressed. Another estimation of higher order effects can be done, as we explained above, by completely neglecting the imaginary part of the matrix elements (c). This suppresses Rea_0 by a factor of $\cos\delta_0^{\rm exp} \simeq 0.8$ but does not affect Rea_2. Similarly the absolute value of the amplitudes can be calculated by taking directly the imaginary part from Tables 3 and 4 without using the experimental phases (d). This procedure suppresses Rea_0 in the same way as in the previous case but largely re-stabilizes Rea_2, indicating that the results obtained for the $\Delta I = 3/2$ amplitude (unlike those obtained for Rea_0) indeed can be significantly affected by higher orders corrections. It is un-

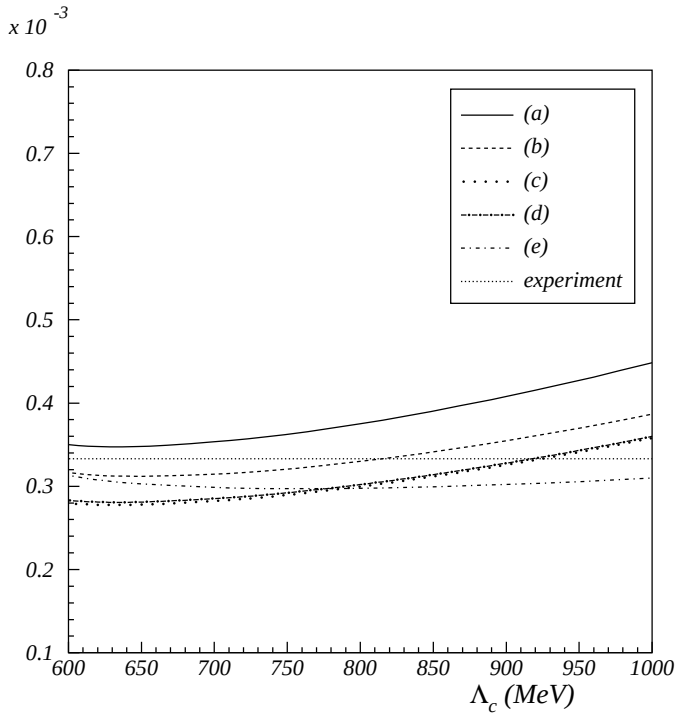

Fig. 8. Rea_0 (in units of MeV) with LO z_i for $m_s(1\,\mathrm{GeV}) = 175\,\mathrm{MeV}$ and $\Lambda_{\overline{\mathrm{MS}}} = 325\,\mathrm{MeV}$ within different treatments of higher order corrections as explained in the text

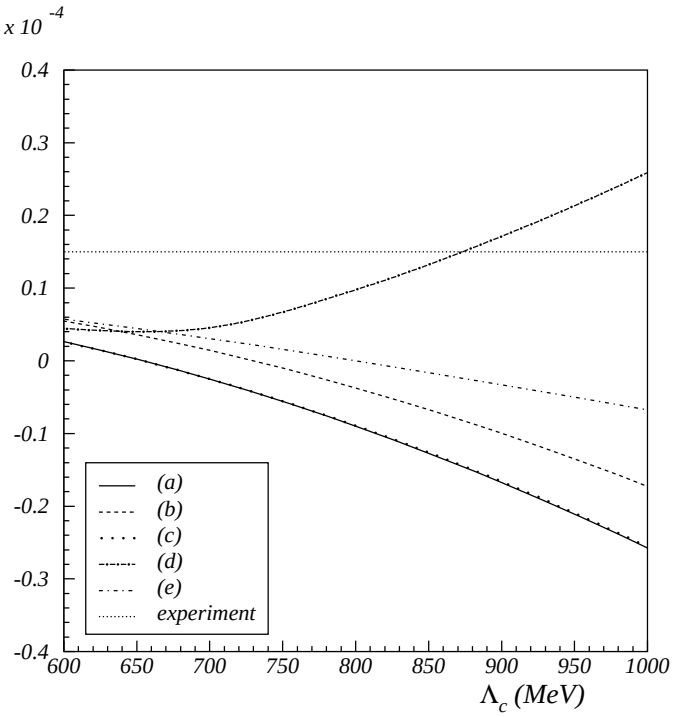

Fig. 9. Rea_2 (in units of MeV) with LO z_i for $\Lambda_{\overline{\mathrm{MS}}} = 325\,\mathrm{MeV}$ within different treatments of higher order corrections as explained in the text

likely, however, that higher order terms alone can account for the large discrepancy between our result and experiment, and effects from higher resonances are also expected to be non-negligible for the small $\Delta I = 3/2$ amplitude. Finally, the coefficient $1/F_\pi$ in the next-to-leading order terms can also be replaced by the bare coupling $1/f$ as was done in [18]. Even though this would introduce an unphysical dependence on the factorizable scale, formally the difference also concerns higher order effects.[11] We observe that this choice (e) leads to a result for Rea_0 which is approximately scale independent. It also gives a more stable result for Rea_2 which, however, still is too much suppressed.

In summary, in all cases we discussed above the $\Delta I = 1/2$ amplitude is obtained around the measured value with an uncertainty of less than 25% or in most cases even less than 15%.[12] The result for Rea_0 is consequently solid and presumably could be significantly affected only by higher resonances. In view of the good agreement with the experiment we obtained at the pseudoscalar level their effect a priori is expected to be small. The $\Delta I = 3/2$ amplitude, on the other hand, though showing the qualitatively correct behavior of being suppressed with respect to the VSA result, emerges too much suppressed and is very unstable. However, higher order corrections to the matrix elements have been estimated large and could re-enhance it. In the same way higher resonances could easily enhance the result obtained at the pseudoscalar level. Vector mesons can be incorporated in a straightforward (however lengthy) way, and it would be very interesting to investigate their effect in the present calculation. This also would allow more safely to choose higher values for the matching scale for which the short-distance contributions are more reliable.

We close this section by a brief review of several other attempts which have been made to explain the $\Delta I = 1/2$ rule using different methods for the computation of the hadronic matrix elements. Interesting tendencies for an enhancement of the $\Delta I = 1/2$ channel were found in particular in [11] by integrating out the quark fields in a gluonic background and in [12] in the framework of QCD sum rules at the level of the inclusive two-point function. In [13] quantitative results reproducing both the $\Delta I = 1/2$ and $\Delta I = 3/2$ channels were obtained adopting the point of view that in addition to $1/N_c$ effects due to one-loop corrections (similar to those of Fig. 2) diquark states play an important role. The results for the $\Delta I = 1/2$ amplitude obtained in the present approach suggest that there are no large diquark effects not already taken into account in the $1/N_c$ corrections we calculated. The $\Delta I = 1/2$ rule has also been investigated in the framework of chiral perturbation theory [14] and the chiral quark model [15]. At the present state of these methods the ratio $1/\omega = 22.2$

[11] The relation between F_π and f is given in (62) of [20] and we obtain $f = 105, 112, 120, 128, 136, 145\,\mathrm{MeV}$ for $\Lambda_c = 500, 600, 700, 800, 900, 1000\,\mathrm{MeV}$, respectively

[12] The only exception to this is the case where the large value of $\Lambda_{\overline{\mathrm{MS}}} = 405\,\mathrm{MeV}$ is taken at LO or NLO (HV scheme) using a matching scale as high as $\sim 1\,\mathrm{GeV}$. In this (unfavorable) case the deviation from the observed value can be as large as 35–40%

cannot be predicted but is used to fit parameters of the models. Very recently the matrix elements relevant for the $\Delta I = 1/2$ rule were studied in lattice QCD with improved statistics [16]. The authors used lowest-order chiral perturbation theory to relate the matrix elements $\langle\pi\pi|Q_i|K^0\rangle$ to $\langle\pi^+|Q_i|K^+\rangle$ and $\langle 0|Q_i|K^0\rangle$ calculated on the lattice. The ratio of the amplitudes computed in this way confirms the significant enhancement of the $\Delta I = 1/2$ channel although systematic uncertainties preclude a definite answer. Whereas the $\Delta I = 1/2$ amplitude is obtained larger than the experimental value by approximately 40% (quenched ensemble[13], $\beta = 6.0$) the $\Delta I = 3/2$ amplitude suffers from ambiguities in the choice of the meson mass due to the ignorance of higher order chiral corrections to the relation between $\mathrm{Re}a_2$ and the B_K parameter. Taking the meson mass $M^2 = (m_K^2 + m_\pi^2)/2$ and using the quenched value of B_K in the continuum limit the authors obtain a value for $\mathrm{Re}a_2$ which also over-estimates the data by approximately 40%. The ratio of the amplitudes exhibits a strong dependence on the meson mass (see Fig. 11 of [16]) due to the chiral behavior of $\mathrm{Re}a_2$. In lattice perturbation theory unlike in analytical methods, the matching of the renormalized operators to the Wilson coefficients can be rigorously done, at least in principle (see e.g. [45] and references therein). On the other hand, analytical methods like the $1/N_\mathrm{c}$ approach followed in this paper allow for a direct evaluation of the $K \to \pi\pi$ amplitudes without the need of using reduction formulas to relate these amplitudes to the off-shell $K \to \pi$ amplitudes (for this point see also [46] and references therein).

While this paper was written an analysis of the $\Delta I = 1/2$ rule was published [47] which follows similar lines of thought as our work. In their analysis the authors used the $1/N_\mathrm{c}$ expansion in the chiral limit in the framework of chiral perturbation theory and the extended Nambu–Jona–Lasinio model, respectively. We agree on the coefficients of the quadratically divergent terms in the $1/N_\mathrm{c}$ corrections to the matrix elements quoted therein. In the present analysis we did not investigate the method proposed in [47] to treat the scheme dependence appearing at the next-to-leading logarithmic order.

5 K^0–$\bar{K}^0$ mixing

The contributions of short-distance physics to K^0–$\bar{K}^0$ mixing can be calculated from an effective $\Delta S = 2$ hamiltonian, valid below the charm threshold, in which the heavy degrees of freedom are integrated out [32],

$$\mathcal{H}_\mathrm{eff}^{\Delta S=2} = \mathcal{F}(m_t^2, m_c^2, M_W^2, V_\mathrm{CKM}) G_F^2 \times [\alpha_\mathrm{s}(\mu)]^{-2/9} \left[1 + \frac{\alpha_\mathrm{s}(\mu)}{4\pi} J_3\right] \mathcal{O}_{\Delta S=2}, \quad (39)$$

where $\mathcal{O}_{\Delta S=2}$ is the following four-quark operator:

$$\mathcal{O}_{\Delta S=2} = \bar{s}_\mathrm{L}\gamma^\mu d_\mathrm{L}\bar{s}_\mathrm{L}\gamma_\mu d_\mathrm{L}, \quad (40)$$

[13] Quantitative estimates of quenching effects on the coefficients of the chiral logarithms in the one-loop contributions to the $K \to \pi\pi$ amplitudes were presented in [43,44]. In [43] finite volume effects on the lattice were also investigated

with $\alpha_\mathrm{s}(\mu)$ being the QCD running coupling with three active flavors and J_3 a renormalization scheme dependent coefficient appearing at the next-to-leading logarithmic order. $\mathcal{F}(m_t^2, m_c^2, M_W^2, V_\mathrm{CKM})$ is a known function of the heavy quark masses, the W boson mass, and CKM matrix elements. It incorporates the basic electroweak (box diagram) loop contributions [48] as well as the perturbative QCD effects described through the correction factors η_1, η_2, η_3 which have been calculated at the leading logarithmic [4,49] and the next-to-leading logarithmic order [32,33]. Terms depending on $\alpha_\mathrm{s}(\mu)$ are factored out explicitly to exhibit the renormalization scale (and scheme) dependence of the coefficients which has to cancel the corresponding scale (and scheme) dependence of the hadronic matrix element of $\mathcal{O}_{\Delta S=2}$ [19]. The short-distance hamiltonian for $\Delta S = 2$ transitions in (39) dominates the indirect CP violation in the neutral kaon system parameterized by ε. Contributions to K^0–$\bar{K}^0$ mixing changing strangeness by two units through two $\Delta S = 1$ transitions at long distances which are relevant for the $K_\mathrm{L} - K_\mathrm{S}$ mass difference [29] are not considered in this article.

The hadronic matrix element of $\mathcal{O}_{\Delta S=2}$ is usually parameterized in terms of the B_K parameter which quantifies the deviation from the value obtained in the vacuum saturation approximation:

$$\langle\bar{K}^0|\mathcal{O}_{\Delta S=2}(\mu)|K^0\rangle = B_K(\mu)\langle\bar{K}^0|\mathcal{O}_{\Delta S=2}|K^0\rangle_\mathrm{VSA}, \quad (41)$$

where

$$\langle\bar{K}^0|\mathcal{O}_{\Delta S=2}|K^0\rangle_\mathrm{VSA} = \frac{4}{3} F_K^2 m_K^2. \quad (42)$$

It is convenient to introduce the renormalization group invariant parameter [19,50]

$$\hat{B}_K = B_K(\mu)\,[\alpha_\mathrm{s}(\mu)]^{-2/9}\left[1 + \frac{\alpha_\mathrm{s}(\mu)}{4\pi} J_3\right], \qquad J_3 = \begin{cases} \frac{307}{162}\ (\mathrm{NDR}) \\ \frac{91}{162}\ (\mathrm{HV}) \end{cases}, \quad (43)$$

in which the scale (and scheme) dependences of the long- and short-distance contributions cancel within an exact realization of both perturbative and non-perturbative QCD. However, from the results for the $\Delta I = 3/2$ $K \to \pi\pi$ amplitude discussed in the previous section we do not expect that the $\hat{B}_K$ we will obtain within the pseudoscalar approximation used in the low-energy calculation will exhibit a negligible dependence on the matching scale; the 27-plet operators which induce $\Delta S = 1$ ($\Delta I = 3/2$) and $\Delta S = 2$ transitions are components of the same irreducible tensor under $\mathrm{SU}(3)_\mathrm{L} \times \mathrm{SU}(3)_\mathrm{R}$, that is to say, to leading order in the chiral expansion the K^0–$\bar{K}^0$ amplitude can be related to the $\Delta I = 3/2$ part of the $K \to \pi\pi$ amplitude using SU(3) symmetry [51,52]. Consequently, we expect a similar pattern, i.e., a large negative quadratic term in the $1/N_\mathrm{c}$ corrections to the matrix element which partly cancels the tree level contribution and renders the result more sensitive to corrections from higher order terms and higher resonances. On the other hand, we expect SU(3) breaking effects in $\Delta S = 2$ transitions to be more pronounced than in $\Delta S = 1$ transitions [53]. In the following

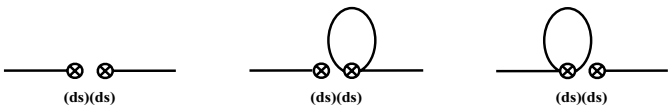

Fig. 10. Factorizable contributions to the matrix element of the K^0–$\bar{K}^0$ mixing amplitude in the isospin limit

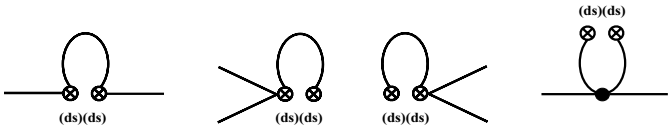

Fig. 11. Non-factorizable contributions to the matrix element of the K^0–$\bar{K}^0$ mixing amplitude in the isospin limit

we will see that the $1/N_c$ expansion restricted to the pseudoscalar mesons indeed leads to a significantly scale dependent result for $\hat{B}_K$. However, the scale dependence is less pronounced than the one of the $\Delta I = 3/2$ amplitude due to corrections beyond the chiral limit. Finally, as we already discussed above, the low-energy calculation does not allow any reference to the renormalization scheme dependence. Nevertheless, a comparison of the $\hat{B}_K$ parameter obtained from the LO and NLO coefficient function of $\mathcal{O}_{\Delta S=2}$ can be used to test the validity of perturbation theory and to estimate the uncertainties arising from the short-distance part.

5.1 Factorizable loop corrections

To obtain the factorizable non-perturbative corrections to the $\Delta S = 2$ transition we have to calculate the diagrams in Fig. 10. Using the chiral representation of the quark current in (16) and reducing the result to the basic integrals listed in Appendix B of [20] we obtain the unrenormalized (bare) matrix element:

$$\begin{aligned}&\langle\bar{K}^0|\mathcal{O}_{\Delta S=2}|K^0\rangle^F_{(0)}\\&= m_K^2 f^2\Bigg[1+\frac{16L_5}{f^2}m_K^2-\frac{1}{9f^2}\Big((a+2b)^2\,I_1[m_\eta]\\&\quad+2\,(a-b)^2\,I_1[m_{\eta'}]+18I_1[m_K]+9I_1[m_\pi]\Big)\Bigg],\end{aligned}\tag{44}$$

with a and b defined in (15). Multiplying (44) with Z_K^{-1}, i.e., including a factor $Z_K^{-1/2}$ for each external kaon field (compare (16) and (59) of [20]), we arrive at

$$\begin{aligned}&\langle\bar{K}^0|\mathcal{O}_{\Delta S=2}|K^0\rangle^F\\&= m_K^2 f^2\Bigg[1+\frac{8L_5}{f^2}m_K^2-\frac{1}{12f^2}\Big(9I_1[m_\pi]+18I_1[m_K]\\&\quad+(a+2b)^2\,I_1[m_\eta]+2\,(a-b)^2\,I_1[m_{\eta'}]\Big)\Bigg].\end{aligned}\tag{45}$$

Comparing (45) with (26) and (63) of [20] we observe that the correction factor in the brackets which is due to the higher order (factorizable) contributions to the matrix element is completely absorbed (including the finite terms) in the renormalization of the kaon decay constant, as is required by current conservation, leading to the final result for the (renormalized) factorizable matrix element

$$\langle\bar{K}^0|\mathcal{O}_{\Delta S=2}|K^0\rangle^F_{(r)} = m_K^2 F_K^2.\tag{46}$$

Equation (46) represents the large-N_c limit for the K^0–$\bar{K}^0$ matrix element, i.e., $B_K^{N_c\to\infty} = 3/4$, to be compared with the VSA value one.

5.2 Non-factorizable loop corrections

The $1/N_c$ corrections to (46) can be calculated from the non-factorizable loop diagrams depicted in Fig. 11. We determine the loop momenta along the lines developed in Sect. 2, that is to say, by associating the cutoff to the effective color singlet boson connecting the two currents. The simple structure of the non-factorizable diagrams makes it possible to specify the complete analytic result for the matrix element in terms of loop integrals. In the SU(2) limit the expression in which the integrals are reduced to the basic ones reads

$$\begin{aligned}&\langle\bar{K}^0|\mathcal{O}_{\Delta S=2}|K^0\rangle^{\mathrm{N}F}\\&=\frac{\Lambda_c^4}{32\pi^2}+\frac{1}{6}\Big(4m_K^2-2p_K^2-(\chi_2+\chi_3)\Big)I_1[m_K]\\&\quad-\frac{1}{6}\big(\chi_2+\chi_3+2m_K^2+2p_K^2\big)m_K^2 I_3[m_K,m_K,0]\\&\quad-\frac{1}{2}(p_K^2+m_\pi^2)I_2[m_\pi,p_K]-\frac{3}{2}\cos^2\theta(p_K^2+m_\eta^2)\\&\quad\times I_2[m_\eta,p_K]-\frac{3}{2}\sin^2\theta(p_K^2+m_{\eta'}^2)I_2[m_{\eta'},p_K]\\&\quad+\frac{1}{4}I_4[m_\pi,p_K]+\frac{3}{4}\cos^2\theta I_4[m_\eta,p_K]\\&\quad+\frac{3}{4}\sin^2\theta I_4[m_{\eta'},p_K].\end{aligned}\tag{47}$$

Here we replaced a and b by the η–η' mixing angle θ and explicitly distinguished between the masses coming from the external kaon momentum, the explicit mass term in the lagrangian, and the propagators in the loops. In addition to the logarithmically and quadratically divergent integrals (I_1, I_2, I_3) listed in Appendix B of [20] (47) contains the integral I_4 which exhibits a quartic dependence on the cutoff. Following the steps discussed in [20] we can give the analytic expression for I_4 in terms of a Taylor-series:

$$\begin{aligned}I_4[m,p] &= \frac{\mathrm{i}}{(2\pi)^4}\int \mathrm{d}^4q\frac{q^2}{(q-p)^2-m^2}\\&=\frac{1}{16\pi^2}\Bigg\{-\frac{1}{2}\Lambda_c^4+m^2\left[\Lambda_c^2-m^2\log\left(1+\frac{\Lambda_c^2}{m^2}\right)\right]\\&\quad+\frac{p^2m^2}{(\Lambda_c^2+m^2)^2}\left[\frac{3}{2}\Lambda_c^4+\Lambda_c^2m^2-(\Lambda_c^2+m^2)^2\right.\end{aligned}$$

$$\times \log\left(1+\frac{\Lambda_c^2}{m^2}\right)\Bigg] + \frac{p^4\Lambda_c^6}{6(\Lambda_c^2+m^2)^4}(\Lambda_c^2-2m^2) + \frac{p^6\Lambda_c^6 m^2}{2(\Lambda_c^2+m^2)^6}\left(\Lambda_c^2-\frac{2}{3}m^2\right)\Bigg\} + \mathcal{O}(p^8). \quad (48)$$

We note that the logarithmically divergent integral I_3 in (47) only appears with vanishing external momentum and therefore can be largely simplified compared to the general expression in (75) of [20]. From (47) one can easily calculate the divergent terms. Taking the external momentum on shell we obtain

$$\langle \bar{K}^0|\mathcal{O}_{\Delta S=2}|K^0\rangle^{\mathrm{NF}} = m_K^2 F_K^2\left[-\frac{3\Lambda_c^2}{(4\pi)^2F_K^2} + \frac{(4m_K^4-2m_K^2m_\pi^2+m_\pi^4)}{(4\pi)^2F_K^2m_K^2}\log\Lambda_c^2+\cdots\right], \quad (49)$$

where the tree level result is factored out and the ellipses denote the finite terms we do not specify analytically. We observe that the quartic dependence on the cutoff is cancelled as required by chiral symmetry.

To illustrate the effect of the modified momentum routing we also recalculate the non-factorizable loop contributions in the approach used by Bardeen et al. [26] who associated the cutoff to the momentum of the virtual meson in the loop diagrams (see also the discussion in [20]):

$$\langle \bar{K}^0|\mathcal{O}_{\Delta S=2}|K^0\rangle^{\mathrm{NF}}_{\mathrm{BBG}} = -\frac{1}{12}\Bigg[2\left(\chi_2+\chi_3-2m_K^2\right)I_1[m_K] + 3\left(m_K^2+m_\pi^2\right)\times I_1[m_\pi] + 9\cos^2\theta\left(m_K^2+m_\eta^2\right)I_1[m_\eta] + 9\sin^2\theta\left(m_K^2+m_{\eta'}^2\right)I_1[m_{\eta'}] + 2m_K^2\left(\chi_2+\chi_3+4m_K^2\right)I_3[m_K,m_K,0]\Bigg], \quad (50)$$

where the external momentum is already taken on shell. For comparison with (47) in (50) we included the small effect of the singlet η_0. Solving the integrals we obtain the divergent part of the non-factorizable loop corrections:

$$\langle \bar{K}^0|\mathcal{O}_{\Delta S=2}|K^0\rangle^{\mathrm{NF}}_{\mathrm{BBG}} = m_K^2 F_K^2\left[-\frac{2\Lambda_c^2}{(4\pi)^2F_K^2} + \frac{(4m_K^4-2m_K^2m_\pi^2+m_\pi^4)}{(4\pi)^2F_K^2m_K^2}\log\Lambda_c^2+\cdots\right], \quad (51)$$

to be compared with (49). We note that the results obtained in both calculations differ with respect to the quadratic cutoff dependence as well as with respect to the finite terms we do not give explicitly here for brevity.

5.3 Numerical results

As a numerical input we use the values listed in Sect. 4.1. In Table 9 we show our results for the K^0–$\bar{K}^0$ matrix element and $B_K(\Lambda_c)$ obtained in the full calculation, i.e., including the effect of the η_0 in (47). In Fig. 12 we depict the renormalization group invariant parameter $\hat{B}_K$ calculated with the leading order Wilson coefficient.

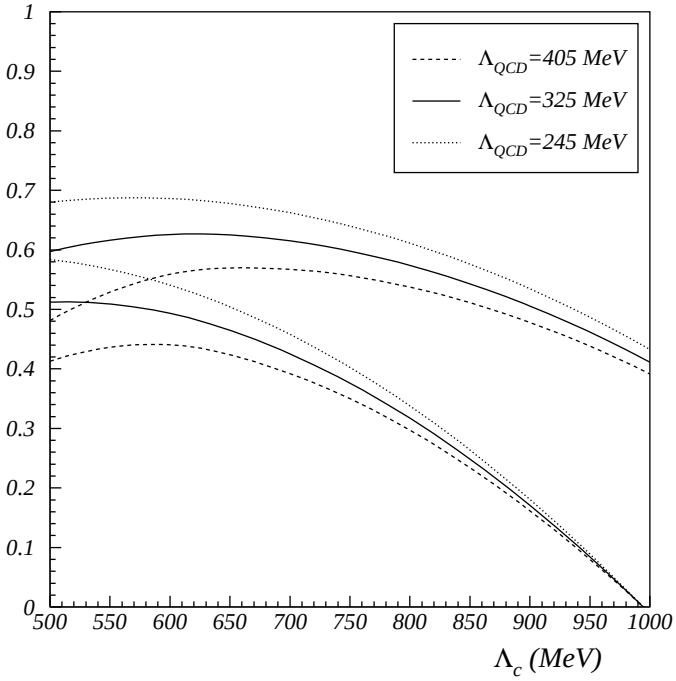

Fig. 12. $\hat{B}_K$ with LO Wilson coefficient for various values of Λ_{QCD} as a function of the matching scale $\Lambda_c = \mu$. The lower set of curves shows the results of the present analysis, the upper set allows a comparison with [26]

The decrease of $B_K(\Lambda_c)$ with $\Lambda_c = \mu$ is qualitatively consistent with the μ dependence of the coefficient function in (43), that is to say, the long-distance evolution counteracts the evolution in the short-distance domain. This property is due to the presence of the quadratic terms in the $1/N_c$ corrections which compensate for the (weaker) increase of the logarithmic terms. However, the decrease is found to be significant, and the scale dependence largely exceeds what is required to have an exact cancellation of both evolutions over a large range of the scale. As a result an acceptable stability of $\hat{B}_K$ is obtained only for low values of $\Lambda_c \simeq 500$–$600\,\mathrm{MeV}$. The small values of $\hat{B}_K$ depicted in Fig. 12 (lower set of curves) come from the negative coefficient of the quadratic term in (49) which is found to be enhanced by a factor of 3/2 compared to the result of [26]. This coefficient is the same as the one of the $\Delta I = 3/2$ $K \to \pi\pi$ amplitude except for SU(3) breaking effects (responsible for $F_K \neq F_\pi$) which reduce the negative slope of $\hat{B}_K$. As can be seen from Table 9, the difference between the exact result and the one obtained in the chiral limit (i.e., in the absence of chiral logarithms and finite terms) is more pronounced than in the case of the $K \to \pi\pi$ amplitudes. This is due mainly to the numerical coefficient of the leading term ($\sim m_K^4$) in front of the logarithm in (49) which, as expected, is found to be larger in $\Delta S = 2$ transitions than in $\Delta S = 1$ transitions. Because of the large positive coef-

Table 9. Different contributions to the hadronic matrix element of $\mathcal{O}_{\Delta S=2}$ (in units of $10^9 \cdot \mathrm{MeV}^4$) and B_K, shown for various values of the cutoff Λ_c

Λ_c	0.5 GeV	0.6 GeV	0.7 GeV	0.8 GeV	0.9 GeV	1.0 GeV
$\langle\mathcal{O}_{\Delta S=2}\rangle_{\mathrm{tree}}$	3.14	3.14	3.14	3.14	3.14	3.14
$\langle\mathcal{O}_{\Delta S=2}\rangle_{\Lambda_c^2}$	−1.17	−1.68	−2.29	−2.99	−3.78	−4.67
$\langle\mathcal{O}_{\Delta S=2}\rangle_{\mathrm{log+fin}}$	0.57	0.76	0.96	1.15	1.32	1.49
$\langle\mathcal{O}_{\Delta S=2}\rangle$	2.54	2.22	1.81	1.30	0.68	−0.04
$B_K(\Lambda_c)$	0.61	0.53	0.43	0.31	0.16	−0.01

ficient the logarithmic term re-stabilizes $\hat{B}_K$ sizably with respect to the result obtained in the chiral limit. This also explains why the $\hat{B}_K$ parameter, even if significantly scale dependent, is much more stable than the $\Delta I = 3/2$ amplitude. The finite terms beyond the logarithms in (47) [i.e., beyond the $\log(1 + \Lambda_c^2/m^2)$ terms] give a negative contribution to $B_K(\Lambda_c)$ roughly between −0.05 and −0.08 for Λ_c around 600–900 MeV. Consequently, they are non-negligible in particular for large values of the scale where the cancellation between the tree level and the quadratic terms is large. Finally, we note that the presence of the η_0 does not significantly affect the numerical values of the K^0–$\bar{K}^0$ matrix element (in the octet limit the numbers given in Table 9 change by less than 3%).

To illustrate the effect of the momentum routing, in Fig. 12 we also show $\hat{B}_K$ obtained from (50) (upper set of curves). We use the same set of parameters as in Table 9 and also include the η_0. Comparing the two results we notice that $B_K(\Lambda_c)$ calculated within the modified momentum routing lies below the values found in the previous approach. Matching the long-distance results with the short-distance contribution we observe that the $\hat{B}_K$ parameter obtained in the present analysis exhibits a significantly stronger dependence on the matching scale. However, as we already discussed above, the quadratically divergent terms (and the finite terms) depend on the way we define the integration variable inside the loop. This can be seen from the different numerical factors in front of the quadratic terms in (49) and (51). Therefore we are forced to find a direct link between the short- and long-distance part of the calculation, as is done by keeping track of the effective color singlet boson in both parts of the calculation. A consistent matching is then obtained by assigning the same momentum to the color singlet boson at long and short distances and by identifying this momentum with the loop integration variable (see Sect. 2). This property is absent in the previous approach. The modification unambiguously determines the coefficient in front of the (quadratically and logarithmically) divergent terms and allows us to identify the ultraviolet cutoff of the long-distance terms with the short-distance renormalization scale μ. Therefore we advocate the use of the modified matching prescription, even though the stability of our result is rather poor. The satisfactory stability obtained in [26] on the other hand is somehow inconclusive, as there is no underlying argumentation determining the quadratic terms. Our result also implies that the uncertainties due to the idealized identification of the cutoff Λ_c with the upper limit of the meson momentum in the loop in [26] might have been underestimated. In a complete meson theory the dependence on the momentum routing should be absent. However, as long as we are working in an effective low-energy approach as chiral perturbation theory we have to pay attention to this point.

Numerically, we find a range of acceptable stability in the energy regime from 500 MeV to 700 MeV (see Fig. 12) leading to values for $\hat{B}_K$ in the range of $0.4 < \hat{B}_K < 0.6$. The lower bound corresponds to a value of $\Lambda_{\mathrm{QCD}} = 405$ MeV, whereas the upper bound corresponds to $\Lambda_{\mathrm{QCD}} = 245$ MeV. Comparing our result with the one of [26] we observe a tendency for $\hat{B}_K$ to be decreased to values below 0.6. This behavior is due to the enhancement of the negative coefficient in front of the quadratic term in the $1/N_c$ corrections to the K^0–$\bar{K}^0$ matrix element and, to a smaller extent, also due to the finite terms omitted in [26]. However, our result suffers from a sizable dependence on the matching scale, which precludes a precise answer.

In Fig. 13 we compare the results for $\hat{B}_K$ we obtain with the LO and the NLO coefficient function. For $\Lambda_{\mathrm{QCD}} = 325$ MeV in the HV scheme, introducing the NLO coefficient does not significantly affect the numerical values of the $\hat{B}_K$ parameter which is found to be only slightly enhanced with respect to the LO result. In the NDR scheme, the effect of the NLO coefficient is also moderate for large values of the scale but noticeably increases for low values. For very low values of $\Lambda_c \simeq 500$ MeV the NLO result can differ from the LO one by as much as 0.2. However, for these scales the scheme dependence increases rapidly and it is desirable to take (at least) a matching scale around 600–650 MeV where $\hat{B}_K$ is still relatively smooth and roughly varies between 0.45 and 0.6. For $\Lambda_{\mathrm{QCD}} = 245$ MeV in both the HV and NDR schemes a matching scale as low as 500 MeV appears to be acceptable, and within the range $\Lambda_c \simeq 500$–650 MeV $\hat{B}_K$ is obtained between 0.5 and 0.7. On the other hand we observe that the pseudoscalar approximation would simply fail if Λ_{QCD} was found as large as 405 MeV, as a satisfactory perturbative behavior is obtained only for $\Lambda_c \gtrsim 700$ MeV, that is to say, for values of the scale where the stability of $\hat{B}_K$ is found to be poor.

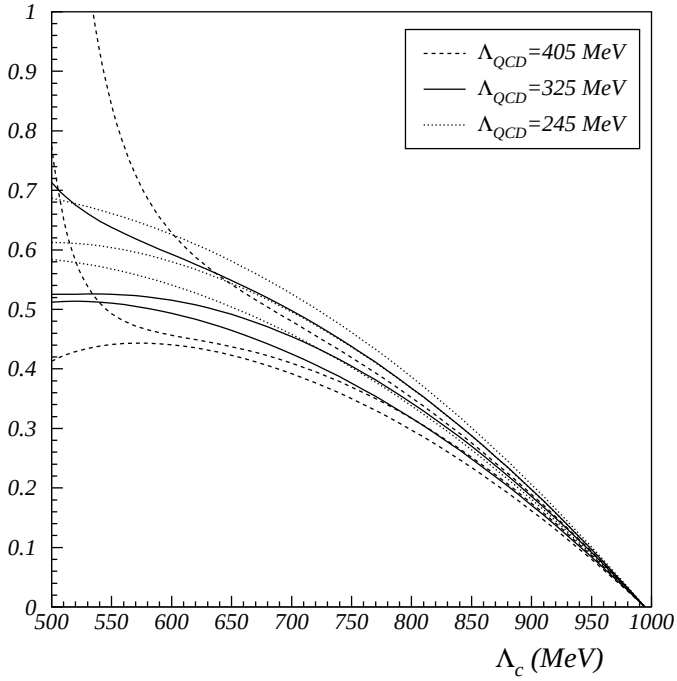

Fig. 13. $\hat{B}_K$ with LO and NLO Wilson coefficient for various values of $\Lambda_{\rm QCD} = \Lambda^{(4)}_{\overline{\rm MS}}$ as a function of the matching scale $\Lambda_c = \mu$. For each value of $\Lambda_{\rm QCD}$ the lower (intermediate, upper) curve shows the LO (HV, NDR) result

In summary, for values of $\Lambda_{\rm QCD} \gtrsim 350\,{\rm MeV}$ an estimate of $\hat{B}_K$ is hindered by the loss of perturbativity in the range where the pseudoscalar approximation is expected to be valid, and for lower values of $\Lambda_{\rm QCD}$ (taking into account the scheme dependence) our calculation favors low values of $\hat{B}_K$ in the range

$$0.4 < \hat{B}_K < 0.7. \tag{52}$$

However, a satisfactory smooth behavior is obtained only in a narrow range of the cutoff and, in addition, for values of the cutoff as low as the kaon mass or just above. Therefore the incorporation of higher resonances is clearly required as for the $\Delta I = 3/2$ $K \to \pi\pi$ amplitude discussed above. On this issue, the analysis of the $\hat{B}_K$ parameter is similar to the one of the $\Delta I = 3/2$ amplitude, even if numerically the matching obtained for $\hat{B}_K$ is better than the one obtained for the $\Delta I = 3/2$ amplitude.

The K^0–$\bar{K^0}$ system has been studied in the past with various methods leading to different results for $\hat{B}_K$. The present status of quenched lattice calculations [54–57] has been reviewed in [58]. The value reported by the author is $\hat{B}_K = 0.86 \pm 0.06 \pm 0.06$. Very recently the JLQCD Collaboration has presented a new analysis based on chiral Ward identities to non-perturbatively determine the mixing coefficients of the $\Delta S = 2$ operator [59]. The numerical results given in [59] are in agreement with the lattice calculations quoted above. In the chiral quark model a value as high as $\hat{B}_K = 1.1 \pm 0.2$ has been obtained [15]. Lower values for $\hat{B}_K$ have been found in the QCD hadronic duality approach [60] ($\hat{B}_K = 0.39 \pm 0.10$), by using SU(3) symmetry and PCAC [51] ($\simeq 1/3$), or using chiral perturbation theory at next-to-leading order [61] (0.42 ± 0.06). QCD sum rules give results around $\hat{B}_K = 0.5$–0.6 with errors in the range of 0.2–0.3 [62,63]. One might note that a value for $\hat{B}_K$ significantly below 0.7 requires simultaneously high values of $|V_{ub}/V_{cb}|$ and $|V_{cb}|$ to be able to fit the experimental value of ε [19]. Finally, we note that the $\hat{B}_K$ parameter was also investigated in the framework of the $1/N_{\rm c}$ expansion in [50]. In this work the matching was not performed at the level of the K^0–$\bar{K}^0$ matrix element but at the level of a related 2-point Green function. Numerically, the matching was found to be unsatisfactory. We agree with this conclusion, as we discussed above, although in [50] the quadratic dependence on the UV cutoff was obtained in disagreement with the present analysis due to the use of a different momentum routing. This has been corrected very recently in [47], and we agree with the results for the $1/N_{\rm c}$ corrections to the K^0–$\bar{K}^0$ matrix element obtained there in the chiral limit. In the present paper we investigated the corrections beyond the chiral limit and found that they are sizable. On the other hand, the authors of [47] investigated higher order corrections calculated in the framework of the extended Nambu–Jona–Lasinio model. As a result they obtained a better stability of the $\hat{B}_K$ parameter. This shows that corrections from higher order terms and higher resonances are expected to be large. Nevertheless the values of $\hat{B}_K$ we obtained in this analysis by performing a full calculation at the pseudoscalar level are meaningful and can be considered as reference values for further investigations incorporating the effects of higher resonances.

6 Conclusions

The $1/N_{\rm c}$ approach developed in [18,26] when modified along the lines of [20] leads to interesting results in the current–current sector of the $\Delta S = 1$ and in the $\Delta S = 2$ transitions. The main result of the present analysis is an additional enhancement of the $\Delta I = 1/2$ channel in the $K \to \pi\pi$ amplitudes. This channel has been found sufficiently enhanced, in good agreement (with an accuracy of 80 to approximately 100%) with the experiment, and widely stable over a large range of values of the matching scale roughly between 600 MeV and 900 MeV. It is certainly premature to say that the dynamical mechanism behind the $\Delta I = 1/2$ enhancement is completely understood. An agreement at the level obtained in the present analysis a priori is not expected in an effective theory with only pseudoscalar mesons taken into account. Nevertheless we believe that the additional enhancement reported here is a further important indication that the $1/N_{\rm c}$ approach can account for the bulk of the $\Delta I = 1/2$ amplitude. This statement is also supported by the fact that higher order corrections both of short-distance origin and of long-distance origin at the pseudoscalar level, as we discussed above, are not expected to largely affect the size of the $\Delta I = 1/2$ enhancement. The agreement with the

experiment also tends to show that the origin of the long-distance enhancement has to be found at the level of the pseudoscalar mesons and at energies below the rho mass or even below the kaon mass. Certainly this has to be checked explicitly incorporating at least the effects of vector mesons. We also believe that the $1/N_c$ approach can account for the bulk of the suppression of the $\Delta I = 3/2$ channel. For this channel, however, the approximations made in the present analysis fell short of the desired accuracy. In particular, a large scale dependence has been found clearly requiring the incorporation of higher order terms and/or higher resonances. We note that the scale behavior of the ratio of the two isospin amplitudes is dominated by the one of the $\Delta I = 3/2$ channel, and therefore it leads to a comparable uncertainty. Similarly, the $\hat{B}_K$ parameter suffers from a sizable dependence on the matching scale. Our calculation favors very low values of the scale ($\lesssim 700\,\text{MeV}$) leading to values for $\hat{B}_K$ in the range of $0.4 < \hat{B}_K < 0.7$. However, the large uncertainties associated with this result preclude a definite answer, and also make the incorporation of higher order terms and higher resonances very desirable.

Acknowledgements. We wish to thank Emmanuel Paschos for many valuable discussions. We also thank William Bardeen, Johan Bijnens, Jorge Fatelo, Jean-Marc Gérard, and Gino Isidori for helpful comments. We are very thankful to Matthias Jamin for providing us with the numerical values of the Wilson coefficients used in Sect. 4 of this article. This work was supported in part by the Bundesministerium für Bildung, Wissenschaft, Forschung und Technologie (BMBF), 057D093P(7), Bonn, FRG, and DFG Antrag PA-10-1.

A Numerical values of the Wilson coefficients

In this appendix we list the numerical values of the LO and NLO (HV and NDR) Wilson coefficients for the $\Delta S = 1$ transitions used in Sect. 4.2. These values were supplied to us by M. Jamin. Following the lines of [5] the coefficients z_i are given for a 10-dimensional operator basis $\{Q_1, \ldots, Q_{10}\}$. Below the charm threshold the set of operators reduces to seven linearly independent operators [see (4)–(7)] with

$$Q_4 = -Q_1 + Q_2 + Q_3, \quad Q_9 = \frac{3}{2}Q_1 - \frac{1}{2}Q_3,$$
$$Q_{10} = \frac{1}{2}Q_1 + Q_2 - \frac{1}{2}Q_3. \tag{53}$$

At next-to-leading logarithmic order in (renormalization group improved) perturbation theory the relations in (53) receive $\mathcal{O}(\alpha_s)$ and $\mathcal{O}(\alpha)$ corrections [5,19]. In the present analysis we use the linear dependence at the level of the matrix elements $\langle Q_i \rangle_I$, i.e., at the level of the pseudoscalar representation where modifications to the relations in (53) are absent. We note that the effect of the different treatment of the operator relations at next-to-leading logarithmic order, which is due to the fact that in the long-distance

Table 10. $\Delta S = 1$ LO Wilson coefficients for $\Lambda_{\text{QCD}} = 245\,\text{MeV}$

μ	0.6 GeV	0.7 GeV	0.8 GeV	0.9 GeV	1.0 GeV
z_1	−0.937	−0.826	−0.748	−0.690	−0.645
z_2	1.576	1.491	1.433	1.391	1.359
z_3	0.016	0.011	0.007	0.005	0.003
z_4	−0.037	−0.027	−0.019	−0.014	−0.009
z_5	0.011	0.008	0.006	0.004	0.003
z_6	−0.045	−0.031	−0.021	−0.015	−0.010
z_7/α	0.023	0.017	0.012	0.008	0.005
z_8/α	0.007	0.004	0.002	0.001	0.0004
z_9/α	0.027	0.019	0.013	0.009	0.006
z_{10}/α	−0.006	−0.003	−0.002	−0.001	−0.0004

Table 11. $\Delta S = 1$ LO Wilson coefficients for $\Lambda_{\text{QCD}} = 325\,\text{MeV}$

μ	0.6 GeV	0.7 GeV	0.8 GeV	0.9 GeV	1.0 GeV
z_1	−1.192	−1.010	−0.893	−0.811	−0.748
z_2	1.779	1.632	1.541	1.479	1.433
z_3	0.025	0.016	0.010	0.007	0.004
z_4	−0.054	−0.036	−0.026	−0.018	−0.012
z_5	0.015	0.011	0.008	0.006	0.004
z_6	−0.070	−0.044	−0.029	−0.019	−0.013
z_7/α	0.033	0.023	0.017	0.012	0.008
z_8/α	0.012	0.006	0.003	0.001	0.001
z_9/α	0.040	0.027	0.019	0.013	0.008
z_{10}/α	−0.010	−0.005	−0.003	−0.001	−0.001

Table 12. $\Delta S = 1$ LO Wilson coefficients for $\Lambda_{\text{QCD}} = 405\,\text{MeV}$

μ	0.6 GeV	0.7 GeV	0.8 GeV	0.9 GeV	1.0 GeV
z_1	−1.576	−1.246	−1.065	−0.947	−0.861
z_2	2.104	1.824	1.676	1.582	1.517
z_3	0.041	0.023	0.014	0.009	0.006
z_4	−0.082	−0.051	−0.034	−0.023	−0.015
z_5	0.022	0.015	0.010	0.007	0.005
z_6	−0.119	−0.066	−0.041	−0.026	−0.016
z_7/α	0.044	0.031	0.022	0.015	0.010
z_8/α	0.024	0.010	0.005	0.002	0.001
z_9/α	0.056	0.037	0.025	0.017	0.011
z_{10}/α	−0.017	−0.008	−0.004	−0.002	−0.001

Table 13. $\Delta S = 1$ NLO Wilson coefficients (NDR) for $\Lambda_{\rm QCD} = \Lambda^{(4)}_{\overline{\rm MS}} = 245\,{\rm MeV}$

μ	0.6 GeV	0.7 GeV	0.8 GeV	0.9 GeV	1.0 GeV
z_1	−0.668	−0.578	−0.516	−0.470	−0.435
z_2	1.391	1.326	1.282	1.252	1.229
z_3	0.038	0.023	0.016	0.012	0.009
z_4	−0.088	−0.059	−0.043	−0.032	−0.025
z_5	0.007	0.009	0.008	0.007	0.006
z_6	−0.102	−0.064	−0.044	−0.032	−0.025
z_7/α	0.018	0.012	0.008	0.006	0.005
z_8/α	0.069	0.039	0.024	0.015	0.009
z_9/α	0.045	0.029	0.020	0.014	0.010
z_{10}/α	−0.032	−0.021	−0.014	−0.009	−0.006

Table 14. $\Delta S = 1$ NLO Wilson coefficients (HV) for $\Lambda_{\rm QCD} = \Lambda^{(4)}_{\overline{\rm MS}} = 245\,{\rm MeV}$

μ	0.6 GeV	0.7 GeV	0.8 GeV	0.9 GeV	1.0 GeV
z_1	−0.898	−0.739	−0.644	−0.579	−0.531
z_2	1.569	1.444	1.373	1.326	1.292
z_3	0.033	0.019	0.012	0.007	0.005
z_4	−0.060	−0.038	−0.025	−0.017	−0.011
z_5	0.012	0.008	0.006	0.004	0.003
z_6	−0.060	−0.036	−0.024	−0.016	−0.010
z_7/α	−0.005	−0.005	−0.004	−0.004	−0.003
z_8/α	0.046	0.027	0.017	0.011	0.007
z_9/α	0.023	0.012	0.006	0.003	0.001
z_{10}/α	−0.038	−0.024	−0.016	−0.010	−0.007

Table 15. $\Delta S = 1$ NLO Wilson coefficients (NDR) for $\Lambda_{\rm QCD} = \Lambda^{(4)}_{\overline{\rm MS}} = 325\,{\rm MeV}$

μ	0.6 GeV	0.7 GeV	0.8 GeV	0.9 GeV	1.0 GeV
z_1	−0.805	−0.712	−0.623	−0.558	−0.509
z_2	1.495	1.424	1.359	1.312	1.278
z_3	0.095	0.046	0.027	0.018	0.013
z_4	−0.193	−0.104	−0.068	−0.048	−0.035
z_5	−0.019	0.005	0.009	0.009	0.008
z_6	−0.261	−0.121	−0.072	−0.049	−0.035
z_7/α	0.039	0.025	0.018	0.014	0.011
z_8/α	0.181	0.079	0.042	0.024	0.014
z_9/α	0.086	0.054	0.036	0.025	0.018
z_{10}/α	−0.056	−0.034	−0.021	−0.013	−0.008

Table 16. $\Delta S = 1$ NLO Wilson coefficients (HV) for $\Lambda_{\rm QCD} = \Lambda^{(4)}_{\overline{\rm MS}} = 325\,{\rm MeV}$

μ	0.6 GeV	0.7 GeV	0.8 GeV	0.9 GeV	1.0 GeV
z_1	−1.381	−1.011	−0.827	−0.716	−0.640
z_2	1.982	1.662	1.513	1.427	1.370
z_3	0.090	0.040	0.022	0.013	0.007
z_4	−0.129	−0.068	−0.041	−0.026	−0.016
z_5	0.016	0.011	0.008	0.006	0.004
z_6	−0.137	−0.066	−0.038	−0.024	−0.014
z_7/α	−0.008	−0.003	−0.002	−0.002	−0.002
z_8/α	0.107	0.050	0.027	0.016	0.010
z_9/α	0.052	0.027	0.015	0.009	0.005
z_{10}/α	−0.077	−0.042	−0.025	−0.016	−0.010

Table 17. $\Delta S = 1$ NLO Wilson coefficients (NDR) for $\Lambda_{\rm QCD} = \Lambda^{(4)}_{\overline{\rm MS}} = 405\,{\rm MeV}$

μ	0.6 GeV	0.7 GeV	0.8 GeV	0.9 GeV	1.0 GeV
z_1	−0.176	−0.795	−0.738	−0.657	−0.592
z_2	0.911	1.485	1.444	1.384	1.336
z_3	0.350	0.108	0.052	0.030	0.019
z_4	−0.637	−0.218	−0.117	−0.074	−0.050
z_5	−0.318	−0.027	0.004	0.009	0.009
z_6	−1.172	−0.288	−0.132	−0.077	−0.050
z_7/α	0.119	0.042	0.029	0.023	0.018
z_8/α	0.699	0.185	0.081	0.042	0.023
z_9/α	0.132	0.089	0.059	0.040	0.029
z_{10}/α	−0.077	−0.054	−0.033	−0.020	−0.012

Table 18. $\Delta S = 1$ NLO Wilson coefficients (HV) for $\Lambda_{\rm QCD} = \Lambda^{(4)}_{\overline{\rm MS}} = 405\,{\rm MeV}$

μ	0.6 GeV	0.7 GeV	0.8 GeV	0.9 GeV	1.0 GeV
z_1	−2.603	−1.494	−1.102	−0.901	−0.778
z_2	3.138	2.084	1.739	1.573	1.475
z_3	0.370	0.102	0.044	0.023	0.012
z_4	−0.403	−0.140	−0.072	−0.042	−0.025
z_5	0.035	0.014	0.010	0.007	0.005
z_6	−0.463	−0.141	−0.067	−0.037	−0.021
z_7/α	−0.063	−0.009	−0.002	−0.001	−0.001
z_8/α	0.342	0.105	0.048	0.026	0.014
z_9/α	0.111	0.051	0.028	0.016	0.009
z_{10}/α	−0.179	−0.078	−0.042	−0.024	−0.014

part there is no (perturbative) counting in α_s, is numerically negligible.

The following parameters are used for the calculation of the Wilson coefficients:

$$M_W = 80.2\,\text{GeV}, \quad \sin^2\theta_W = 0.23, \quad \alpha = 1/129,$$
$$m_t = 170\,\text{GeV}, \quad \overline{m}_b(m_b) = 4.4\,\text{GeV},$$
$$\overline{m}_c(m_c) = 1.3\,\text{GeV}.$$

References

1. M. Gell-Mann, A. Pais, Proceeding Glasgow Conference 1954 (Pergamon, London 1954), p. 342; R.W. Birge et al., Nuovo Cimento **4**, 834 (1956); G. Alexander et al., Nuovo Cimento **6**, 478 (1957)
2. M.K. Gaillard, B.W. Lee, Phys. Rev. Lett. **33**, 108 (1974); G. Altarelli, L. Maiani, Phys. Lett. B **52**, 351 (1974)
3. M.A. Shifman, A.I. Vainshtein, V.I. Zakharov, Nucl. Phys. B 120 (1977) 316; JETP Lett. **45**, 670 (1977)
4. F.J. Gilman, M.B. Wise, Phys. Rev. D **20**, 2392 (1979); ibid. D **27**, 1128 (1983); B. Guberina, R.D. Peccei, Nucl. Phys. B **163**, 289 (1980).
5. A.J. Buras, M. Jamin, M.E. Lautenbacher, P.H. Weisz, Nucl. Phys. B 400, **37**, 75 (1993); A.J. Buras, M. Jamin, M.E. Lautenbacher, Nucl. Phys. B **408**, 209 (1993)
6. M. Ciuchini, E. Franco, G. Martinelli, L. Reina, Phys. Lett. B **301**, 263 (1993)
7. J. Bijnens, M.B. Wise, Phys. Lett. B **137**, 245 (1984).
8. A.J. Buras, J.-M. Gérard, Phys. Lett. B 192, 1(1987) 56.
9. W.A. Bardeen, A.J. Buras, J.-M. Gérard, Phys. Lett. B 180 (1986) 133; Nucl. Phys. B **293**, 787 (1987)
10. B.W. Lee, J.R. Primack, S.B. Treiman, Phys. Rev. D **7**, 510 (1973); M.K. Gaillard, B.W. Lee, Phys. Rev. D **10**, 897 (1974)
11. A. Pich, E. de Rafael, Nucl. Phys. B **358**, 311 (1991)
12. M. Jamin, A. Pich, Nucl. Phys. B **425**, 15 (1994)
13. M. Neubert, B. Stech, Phys. Rev. D **44**, 775 (1991)
14. J. Kambor, J. Missimer, D. Wyler, Nucl. Phys. B **346**, 17 (1990); Phys. Lett. B **261**, 496 (1991)
15. S. Bertolini, J.O. Eeg, M. Fabbrichesi, E.I. Lashin, Nucl. Phys. B **514**, 63 (1998).
16. D. Pekurovsky, G. Kilcup, talk given at the 16th International Symposium on Lattice Field Theory (Lattice 98), Boulder, CO, 13–18 July 1998, eprint hep-lat/9809115; eprint hep-lat/9812019 (submitted to Phys. Rev. D)
17. G. 't Hooft, Nucl. Phys. B **72**, 461 (1974); Nucl. Phys. B **75**, 461 (1974)
18. W.A. Bardeen, A.J. Buras, J.-M. Gérard, Phys. Lett. B 192 (1987) 138; A.J. Buras, in CP Violation, ed. C. Jarlskog, World Scientific, **5** 75 (1989)
19. G. Buchalla, A.J. Buras, M.E. Lautenbacher, Rev. Mod. Phys. **68**, 1125 (1996)
20. T. Hambye, G.O. Köhler, E.A. Paschos, P.H. Soldan, W.A. Bardeen, Phys. Rev. D **58**, 014017 (1998)
21. T. Hambye, talk given at 21st International School of Theoretical Physics (USTRON 97), Ustron, Poland, 19–24 September 1997, published in Acta Phys. Polon. B **28**, 2479 (1997)
22. G.O. Köhler, talk given at 16th Autumn School and Workshop on Fermion Masses, Mixing and CP Violation (CPMASS 97), Lisbon, Portugal, 6–15 October 1997 (hep-ph/9806224)
23. T. Hambye, P. Soldan, talk given at 16th Autumn School and Workshop on Fermion Masses, Mixing and CP Violation (CPMASS 97), Lisbon, Portugal, 6–15 October 1997 (hep-ph/9806203)
24. J. Gasser, H. Leutwyler, Nucl. Phys. B **250**, 465 (1985)
25. J.-M. Gérard, Mod. Phys. Lett. A **5**, 391 (1990)
26. W.A. Bardeen, A.J. Buras, J.-M. Gérard, Phys. Lett. B **211**, 343 (1988)
27. J. Heinrich, E.A. Paschos, J.-M. Schwarz, Y.L Wu, Phys. Lett. B **279**, 140 (1992); E.A. Paschos, Invited Talk presented at the 27th Lepton–Photon Symposium, Beijing, China (August 1995), published in Lepton/Photon Symposium 1995
28. W.A. Bardeen, talk presented at the Workshop on Hadronic Matrix Elements and Weak Decays, Ringberg Castle, Germany (April 1988), published in Nucl. Phys. Proc. Suppl. 7A, 1 (1989) 49
29. J. Bijnens, J.-M. Gérard, G. Klein, Phys. Lett. B **257**, 191 (1991)
30. J.P. Fatelo, J.-M. Gérard, Phys. Lett. B **347**, 136 (1995)
31. P.H. Soldan, Invited talk presented at the Workshop on K Physics, Orsay, France, May 30–June 4, 1996; published in the proceedings (hep-ph/9608281)
32. A.J. Buras, M. Jamin, P.H. Weisz, Nucl. Phys. B **347**, 491 (1990)
33. S. Herrlich, U. Nierste, Nucl. Phys. B **419**, 292 (1994); Phys. Rev. D **52**, 6505 (1995); Nucl. Phys. B **476**, 27 (1996)
34. A.J. Buras, eprint hep-ph/9806471, to appear in 'Probing the Standard Model of Particle Interactions', edited by F. David, R. Gupta, (Elsevier Science, Amsterdam 1998)
35. I. Gerstein, R. Jackiw, B.W. Lee, S. Weinberg, Phys. Rev. D **3**, 2486 (1971)
36. C. Caso et al. (Particle Data Group), Eur. Phys. J. C **3**, 1 (1998)
37. T. Hambye, G.O. Köhler, E.A. Paschos, P.H. Soldan, in preparation
38. M. Knecht, S. Peris, E. de Rafael, eprint hep-ph/9812471
39. M. Knecht, S. Peris, E. de Rafael, Phys. Lett. B **443**, 255 (1998); S. Peris, M. Perrottet, E. de Rafael, J. High Energy Phys. 9805:0 (1998) 11
40. S. Bertolini, J.O. Eeg, M. Fabbrichesi, eprint hep-ph/9802405
41. J.L. Basdevant, C.D. Froggatt, J.L. Petersen, Nucl. Phys. B **72**, 413 (1974); J.L. Basdevant, P. Chapelle, C. Lopez, M. Sigelle, Nucl. Phys. B **98**, 285 (1975); C.D. Froggatt, J.L. Petersen, Nucl. Phys. B **129**, 89 (1977).
42. S. Bertolini, J.O. Eeg, M. Fabbrichesi, E.I. Lashin, Nucl. Phys. B **514**, 93 (1998)
43. M. Golterman, K.C. Leung, Phys. Rev. D **56**, 2950 (1997)
44. E. Pallante, eprint hep-lat/9808018; talk given at 16th International Symposium on Lattice Field Theory (Lattice 98), Boulder, CO, 13–18 July 1998, eprint hep-lat/9810012
45. C. Dawson et al., Nucl. Phys. B **514**, 313 (1998); G. Martinelli, eprint hep-lat/9810013
46. J. Bijnens, E. Pallante, J. Prades, Nucl. Phys. B **521**, 305 (1998)
47. J. Bijnens, J. Prades, eprint hep-ph/9811472 (to appear in JHEP)
48. T. Inami, C.S. Lim, Progr. Theor. Phys. **65**, 297 (1981)
49. W.A. Kaufman, H. Steger, Y.P. Yao, Mod. Phys. Lett. A **3**, 1479 (1989); J.M. Flynn, Mod. Phys. Lett. A **5**, 877

(1990); A. Datta, J. Fröhlich, E.A. Paschos, Z. Phys. C **46**, 63 (1990)
50. J. Bijnens, J. Prades, Nucl. Phys. B **444**, 523 (1995)
51. J.F. Donoghue, E. Golowich, B.R. Holstein, Phys. Lett. B **119**, 412 (1982)
52. J.-M. Gérard, Acta Phys. Polon. B **21**, 257 (1990)
53. J. Bijnens, H. Sonoda, M.B. Wise, Phys. Rev. Lett. **53**, 2367 (1984)
54. G. Kilcup, R. Gupta, S. Sharpe, Phys. Rev. D **57**, 1654 (1998)
55. D. Pekurovsky, G. Kilcup, Nucl. Phys. Proc. Suppl. **63**, 293 (1998)
56. L. Conti et al., Phys. Lett. B **421**, 273 (1998)
57. JLQCD Collaboration (S. Aoki et al.), Phys. Rev. Lett. **80**, 5271 (1998)
58. R. Gupta, Invited talk given at the 16th Autumn School and Workshop on Fermion Masses, Mixing and CP Violation (CPMASS 97), Lisbon, Portugal, 6–15 October 1997 (hep-ph/9801412)
59. JLQCD Collaboration (S. Aoki et al.), eprint hep-lat/9901018
60. A. Pich, E. de Rafael, Phys. Lett. B **158**, 477 (1985); J. Prades et al., Z. Phys. C **51**, 287 (1991)
61. C. Bruno, Phys. Lett. B **320**, 135 (1994)
62. N. Bilic, C.A. Dominguez, B. Guberina, Z. Phys. C **39**, 351 (1988)
63. R. Decker, Nucl. Phys. Proc. Suppl. 7A, 1 (1989) 80; S. Narison, Phys. Lett. B **351**, 369 (1995).